Cell Reports

Article

Npas4 regulates IQSEC3 expression in hippocampal somatostatin interneurons to mediate anxiety-like behavior

Graphical abstract

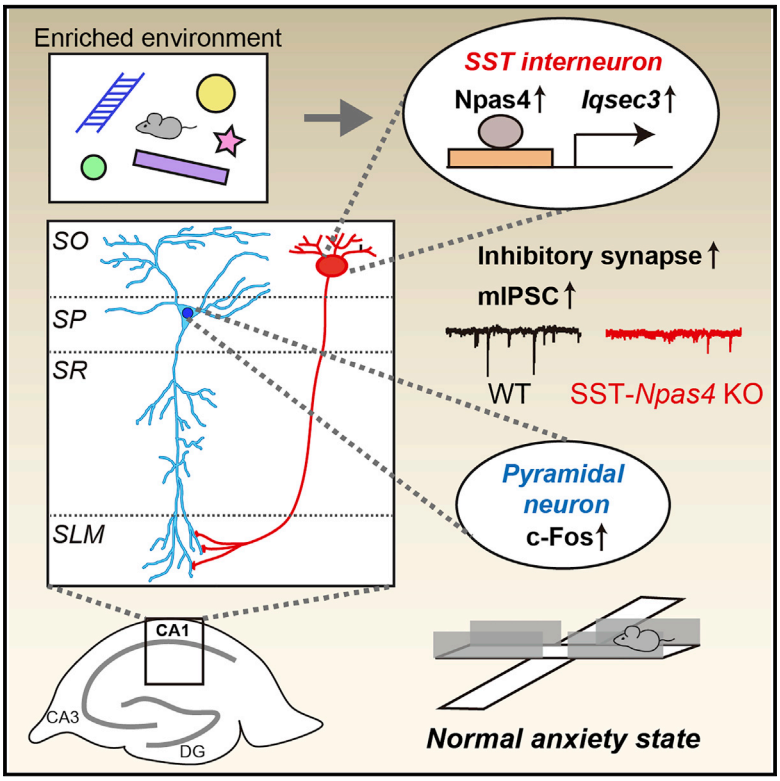

Highlights

- Npas4 binds to the promoter of *IQSEC3* and regulates its expression
- Npas4 upregulates IQSEC3 expression in SST$^+$ interneurons
- Npas4/IQSEC3-dependent inhibition of SST$^+$ interneurons controls anxiety-like behavior
- The ARF-GEF activity of IQSEC3 is critical for its synaptic functions

Authors

Seungjoon Kim, Dongseok Park, Jinhu Kim, ..., Jaehoon Kim, Ji Won Um, Jaewon Ko

Correspondence

jiwonum@dgist.ac.kr (J.W.U.), jaewonko@dgist.ac.kr (J.K.)

In brief

Kim et al. show that IQSEC3 functions as a downstream factor for Npas4 in somatostatin-expressing interneurons of the hippocampal CA1 to mediate neuronal activity-dependent GABAergic synapse organization and proper anxiety-like behavior. The findings reveal the cell-type-specific role of IQSEC3 at hippocampal synapses *in vivo*.

Kim et al., 2021, Cell Reports *36*, 109417
July 20, 2021
https://doi.org/10.1016/j.celrep.2021.109417

CellPress

Cell Reports

CellPress
OPEN ACCESS

Article

Npas4 regulates IQSEC3 expression in hippocampal somatostatin interneurons to mediate anxiety-like behavior

Seungjoon Kim,[1,6] Dongseok Park,[1,6] Jinhu Kim,[1,6] Dongwook Kim,[1] Hyeonho Kim,[1] Takuma Mori,[2] Hyeji Jung,[1] Dongsu Lee,[3] Sookyung Hong,[4] Jongcheol Jeon,[4] Katsuhiko Tabuchi,[2,5] Eunji Cheong,[3] Jaehoon Kim,[4] Ji Won Um,[1,7,8,*] and Jaewon Ko[1,7,*]

[1]Department of Brain and Cognitive Sciences, Daegu Gyeongbuk Institute of Science and Technology (DGIST), 333 Techno Jungangdae-Ro, Hyeonpoong-Eup, Dalseong-Gun, Daegu 42988, Korea
[2]Institute for Biomedical Sciences, Interdisciplinary Cluster for Cutting Edge Research, Shinshu University, Nagano 390-86221, Japan
[3]Department of Biotechnology, College of Life Science and Biotechnology, Yonsei University, Seoul 03722, Korea
[4]Department of Biological Sciences, Korea Advanced Institute of Science and Technology (KAIST), Daejeon 34141, Korea
[5]Department of Molecular and Cellular Physiology, Institute of Medicine, Academic Assembly, Shinshu University, Nagano 390-8621, Japan
[6]These authors contributed equally
[7]Senior author
[8]Lead contact
*Correspondence: jiwonum@dgist.ac.kr (J.W.U.), jaewonko@dgist.ac.kr (J.K.)
https://doi.org/10.1016/j.celrep.2021.109417

SUMMARY

Activity-dependent GABAergic synapse plasticity is important for normal brain functions, but the underlying molecular mechanisms remain incompletely understood. Here, we show that Npas4 (neuronal PAS-domain protein 4) transcriptionally regulates the expression of IQSEC3, a GABAergic synapse-specific guanine nucleotide-exchange factor for ADP-ribosylation factor (ARF-GEF) that directly interacts with gephyrin. Neuronal activation by an enriched environment induces Npas4-mediated upregulation of IQSEC3 protein specifically in CA1 *stratum oriens* layer somatostatin (SST)-expressing GABAergic interneurons. SST^+ interneuron-specific knockout (KO) of Npas4 compromises synaptic transmission in these GABAergic interneurons, increases neuronal activity in CA1 pyramidal neurons, and reduces anxiety behavior, all of which are normalized by the expression of wild-type IQSEC3, but not a dominant-negative ARF-GEF-inactive mutant, in SST^+ interneurons of *Npas4*-KO mice. Our results suggest that IQSEC3 is a key GABAergic synapse component that is directed by Npas4 and ARF activity, specifically in SST^+ interneurons, to orchestrate excitation-to-inhibition balance and control anxiety-like behavior.

INTRODUCTION

An essential function of the nervous system is to generate optimal behavioral responses to diverse environmental information; moreover, combinatorial interactions between genetic components and sensory cues are essential for driving discrete steps in brain development (Chen et al., 2017; Katz and Shatz, 1996; West and Greenberg, 2011; Wong and Ghosh, 2002). Neuronal activity and subsequent calcium influx activate specific signaling cascades that cause the nuclear translocation of various transcription factors, resulting in the rapid induction of an early-response gene-expression program that, in turn, induces the transcription of late-response genes that locally regulate synaptic development and plasticity. Transcription factors commonly induced by synaptic activity regulate distinct sets of target genes to control the strength, location, and number of glutamatergic and GABAergic inputs (Mann and Paulsen, 2007). However, the identity of specific transcription factors that couple with key synapse-organizing proteins to orchestrate the regulation of synapse maintenance and development at both transcriptional and post-transcriptional levels remains unclear (West and Greenberg, 2011).

One prominent transcription factor that specifically controls GABAergic synapse organization is Npas4 (neuronal PAS domain protein 4) (Bloodgood et al., 2013; Kim et al., 2018; Ko et al., 2015; Lin et al., 2008; Spiegel et al., 2014; Sun and Lin, 2016), which is required for neuronal excitability in the adult dentate gyrus (DG) and for new and reactivated fear memories (Ploski et al., 2011; Sim et al., 2013). Npas4 recruits RNA polymerase II to promoters and enhancers of target genes that are regulated by neuronal activity in CA3 hippocampal subfields, thereby contributing to short- and long-term contextual memory (Ramamoorthi et al., 2011). Deletion of *Npas4* abolishes depolarization-induced mRNA expression of immediate-early genes, such as Arc/Arg3.1, c-Fos, Zif268/Egr1, and brain-derived neurotrophic factor (BDNF) (Ramamoorthi et al., 2011). Importantly, Npas4 expression levels dictate the degree of inhibition in specific neuronal compartments by organizing distinct neuron

type-specific genetic programs (Bloodgood et al., 2013; Spiegel et al., 2014). Notably, BDNF regulates somatic, but not dendritic, inhibition in neural circuits of CA1 pyramidal neurons, and is responsive only to increased inhibitory inputs in glutamatergic neurons (Bloodgood et al., 2013; Spiegel et al., 2014). Npas4 mediates experience-dependent spine development in olfactory bulb interneurons through the control of Mdm2 expression, confers neuroprotection against kainic acid (KA)-induced excitotoxicity in hippocampal neurons through the control of synaptotagmin-10 (Syt10) expression, and organizes the structure and strength of hippocampal mossy fiber-CA3 synapses during contextual memory formation through the control of polo-like kinase 2 (Plk2) expression (Weng et al., 2018; Woitecki et al., 2016; Yoshihara et al., 2014). Moreover, in response to heightened neuronal activity, Npas4 is recruited to activity-dependent regulatory elements by ARNT2, which is normally complexed with NCoR2, a co-repressor of neuronal activity-regulated gene expression under basal states (Sharma et al., 2019). These prior studies suggest that synaptic roles of Npas4 vary in a brain region-dependent, a synapse-type-dependent, and a cellular context-dependent manner. Despite these insights, the sheer number of Npas4 target genes has hampered efforts to fully understand the mechanisms underlying Npas4-mediated GABAergic synapse organization. IQSEC3 (IQ motif and Sec7 domain 3; also known as BRAG3 or SynArfGEF) was previously isolated as a putative Npas4 target (Bloodgood et al., 2013). However, direct functional coupling of Npas4 with IQSEC3 in the context of GABAergic synapse organization *in vivo* has not been investigated.

IQSEC3, a member of the brefeldin A-resistant ADP ribosylation factor guanine exchange factor (ARF-GEF) family, is exclusively localized at GABAergic synapses (Fukaya et al., 2011; Sakagami et al., 2013; Um, 2017; Um et al., 2016). IQSEC3 overexpression increases the number of postsynaptic gephyrin and presynaptic GAD67 puncta, whereas IQSEC3 knockdown (KD) specifically decreases gephyrin cluster size in cultured hippocampal neurons, without altering gephyrin puncta density (Um et al., 2016). In addition, IQSEC3 KD in the DG induced severe seizure activity, an effect that was reversed by the restricted expression of somatostatin (SST) peptides in SST^+ interneurons (Kim et al., 2020b) or by reducing microglial activation (Park et al., 2020), suggesting that IQSEC3 may be critical for the maintenance of network activities *in vivo*. However, the brain region-specific, neuronal activity-dependent role of IQSEC3 *in vivo* has yet to be identified.

Here, we provide the evidence demonstrating that IQSEC3 mediates activity-dependent GABAergic synapse number and transmission, coupled with Npas4-dependent transcriptional programs, specifically in SST^+ interneurons. IQSEC3 regulates Npas4-dependent spontaneous GABAergic, but not glutamatergic, synaptic transmission in SST^+ interneurons of the mouse hippocampal CA1 area, and further modulates the activity of CA1 pyramidal neurons, a function that also requires its ARF-GEF activity. Furthermore, the expression of IQSEC3 WT, but not an ARF-GEF activity-deficient IQSEC3 mutant, in SST^+ interneurons restored the altered anxiety-like behaviors observed in conditional knockout (cKO) mice lacking *Npas4* in SST^+ interneurons. Our data suggest that IQSEC3 is a downstream factor for Npas4 in SST^+ interneurons that may sculpt neuronal inhibition onto excitatory neurons, hinting at its crucial roles in shaping activity-dependent specific inhibitory neural circuits and controlling a selective set of mouse behaviors.

RESULTS

Npas4 binds to the *IQSEC3* promoter

The structural and functional plasticity of GABAergic synapses are dynamically modulated in a neuronal activity-dependent manner (Flores and Méndez, 2014; Oh and Smith, 2019). We thus hypothesized that IQSEC3 may be involved in activity-dependent GABAergic synapse organization. Among GABAergic synapse-specific transcription factors, Npas4 appears to be a prominent candidate factor with the potential to play this role (Lin et al., 2008; Shamloo et al., 2006). Npas4 orchestrates the expression of a wide variety of target genes, notably including that encoding BDNF, which regulates GABAergic synapse organization to mediate domain-specific inhibition in particular cell types (Bloodgood et al., 2013; Lin et al., 2008; Spiegel et al., 2014). Intriguingly, deep sequencing of Npas4-bound DNA revealed IQSEC3 as a putative Npas4 target (Bloodgood et al., 2013), and a genome-wide chromatin immunoprecipitation sequencing (ChIP-seq) analysis showed strong enrichment of Npas4 at the upstream region near the transcription start site of the *IQSEC3* gene (Kim et al., 2010) (Figure 1A). Intriguingly, we noted that this Npas4 peak contains a single Npas4 consensus CACG motif (Figure 1A). Thus, we tested whether IQSEC3 could also be an Npas4 target that acts to promote GABAergic synapse organization. To this end, we cotransfected HEK293T cells with a luciferase reporter bearing the *Iqsec3* promoter region in the presence or absence of an Npas4 expression vector. Ectopic expression of Npas4 increased luciferase expression ~3-fold; notably, this increase was abolished by the mutation of the Npas4 consensus site (Figure 1B). We further performed luciferase reporter assays in primary cultured cortical neurons derived from Npas4 floxed mice ($Npas4^{f/f}$) infected with lentiviruses expressing active Cre-recombinase fused to EGFP (Cre) or inactive Cre-recombinase fused to EGFP (ΔCre, as a control) and transfected with an *Iqsec3* promoter-luciferase reporter construct. We found that treatment with 55 mM KCl to trigger membrane depolarization robustly increased the luciferase expression of IQSEC3 by ~3.5 fold and IQSEC3 mRNA levels by ~2.04 fold in control neurons, but that these effects were abolished in Npas4-deficient neurons (Figures 1C and 1D). Electrophoretic mobility shift assays confirmed these results, showing that a radiolabeled *Iqsec3* WT oligoduplex probe containing purified Npas4 protein yielded a single bound complex; consistent with promoter-reporter assays, this DNA-protein interaction was abolished by mutation of the Npas4 consensus site (Figure 1E). ChIP assays also demonstrated that Npas4 binds to the *Iqsec3* promoter in hippocampal cultured neurons treated with 55 mM KCl (Figure 1F). No Npas4-binding was detected in untreated hippocampal cultured neurons (Figure 1F). These data suggest that Npas4 can function as a DNA-binding transcriptional activator of *IQSEC3*.

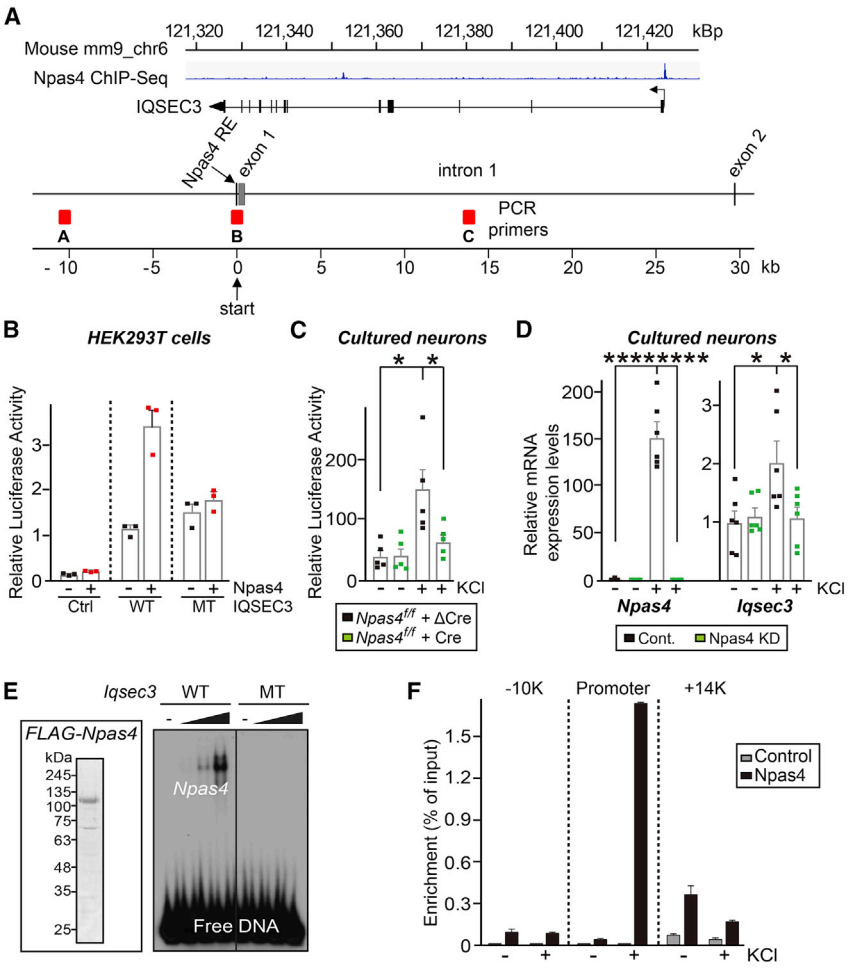

Figure 1. Npas4 binds to the IQSEC3 promoter in an activity-dependent manner

(A) (Top) Localization of Npas4 across the Iqsec3 locus analyzed from the genome-wide ChIP-seq data (Kim et al., 2010). (Bottom) Schematic representation of the Iqsec3 locus indicating the 3 amplicons (A, B, and C) used for ChIP-qPCR analysis in (F). An Npas4-binding site identified by ChIP-seq analysis is indicated as an Npas4 responsive element (Npas4 RE). Data were downloaded from the GEO website (https://www.ncbi.nlm.nih.gov/geo); GEO: GSE21161 (Kim et al., 2010). The total number of tags was normalized to the corresponding input.

(B) HEK293T cells were cotransfected with a luciferase reporter construct (100 ng) containing a *Iqsec3* proximal promoter region (−280 to +36) together with a vector expressing Npas4 (40 ng), as indicated. MT indicates a promoter-reporter construct harboring a mutation in the consensus Npas4-binding sequence. The level of luciferase activity in cells transfected with the WT *Iqsec3* promoter-containing reporter plasmid alone is arbitrarily set at 1. Values are expressed as means ± SEMs from 3 independent experiments.

(C) Cortical cultured neurons derived from Npas4$^{f/f}$ mice were infected with lentiviruses expressing ΔCre or Cre at DIV3 and transfected with a luciferase reporter construct containing an *Iqsec3* proximal promoter region at DIV10. Luciferase activity in extracts of neurons left untreated or treated with 55 mM KCl for 2 h was assayed at DIV10. Values are expressed as means ± SEMs (*$p < 0.05$).

(D) Cortical cultured neurons were infected with lentiviruses expressing shCtrl or shNpas4 at DIV3, treated or untreated with 55 mM KCl, and harvested for quantitative RT-PCR (qRT-PCR) experiments at DIV10. Values are expressed as means ± SEMs (*$p < 0.05$; ****$p < 0.0001$).

(E) Electrophoretic mobility shift assays (EMSAs) using purified FLAG-tagged Npas4 protein (10–90 ng) and a probe corresponding to nucleotide −110 to −69 within the *Iqsec3* proximal promoter are shown. An inset shows an image of a Coomassie Blue-stained SDS-PAGE gel of the purified FLAG-Npas4 protein used in experiments.

(F) ChIP-qPCR analysis of Npas4 localization at the *Iqsec3* locus. Mouse cortical neurons, untreated or treated with 55 mM KCl, were subjected to ChIP analyses with an anti-Npas4 antibody. Error bars denote standard deviations for 3 independent PCR reactions from a single ChIP assay that was representative of several that were performed.

IQSEC3 functions as an Npas4 target to promote GABAergic synapse organization

To further determine whether IQSEC3, analogous to BDNF (Lin et al., 2008), is involved in Npas4 actions on GABAergic synapse organization, we infected cultured neurons with lentiviruses expressing short hairpin RNAs (shRNAs) against *Iqsec3*, *Bdnf*, or control shRNA at 3 days *in vitro* (DIV3), transfected them at DIV10 with EGFP alone or EGFP and myc-Npas4, and then immunostained them at DIV14 for gephyrin. Overexpression of Npas4 significantly increased gephyrin puncta density in both dendrites and somata, an effect that was completely abolished by IQSEC3 KD (Figures 2A–2D). These effects were distinct from the previously reported BDNF KD effects on an Npas4 minigene, which led to altered GABAergic synaptic transmission specifically in the soma, but not in the dendritic compartment (Bloodgood et al., 2013) (Figures 2A–2D). These data suggest that IQSEC3 acts downstream of Npas4 to regulate GABAergic synapse numbers in cultured hippocampal neurons.

To examine whether altered gephyrin puncta size in IQSEC3-deficient cultured hippocampal neurons influences GABAergic synaptic transmission *in vivo*, we performed patch-clamp recordings in CA1 hippocampal pyramidal neurons from mice. Experiments in which mice were electroporated with shRNAs targeting IQSEC3 (shIQSEC3) *in utero* revealed that IQSEC3 KD specifically decreased the frequency, but not the amplitude, of miniature inhibitory postsynaptic currents (mIPSCs) without altering the frequency or amplitude of miniature excitatory postsynaptic currents (mEPSCs; Figures 2E–2K). Importantly, IQSEC3 KD did not alter the paired-pulse ratio of IPSCs (Figures 2L and 2M), suggesting that the IQSEC3 KD-induced reduction in GABAergic synaptic transmission reflects mainly postsynaptic effects. These results suggest that IQSEC3 is required for GABAergic synapse density and transmission in hippocampal CA1 pyramidal neurons.

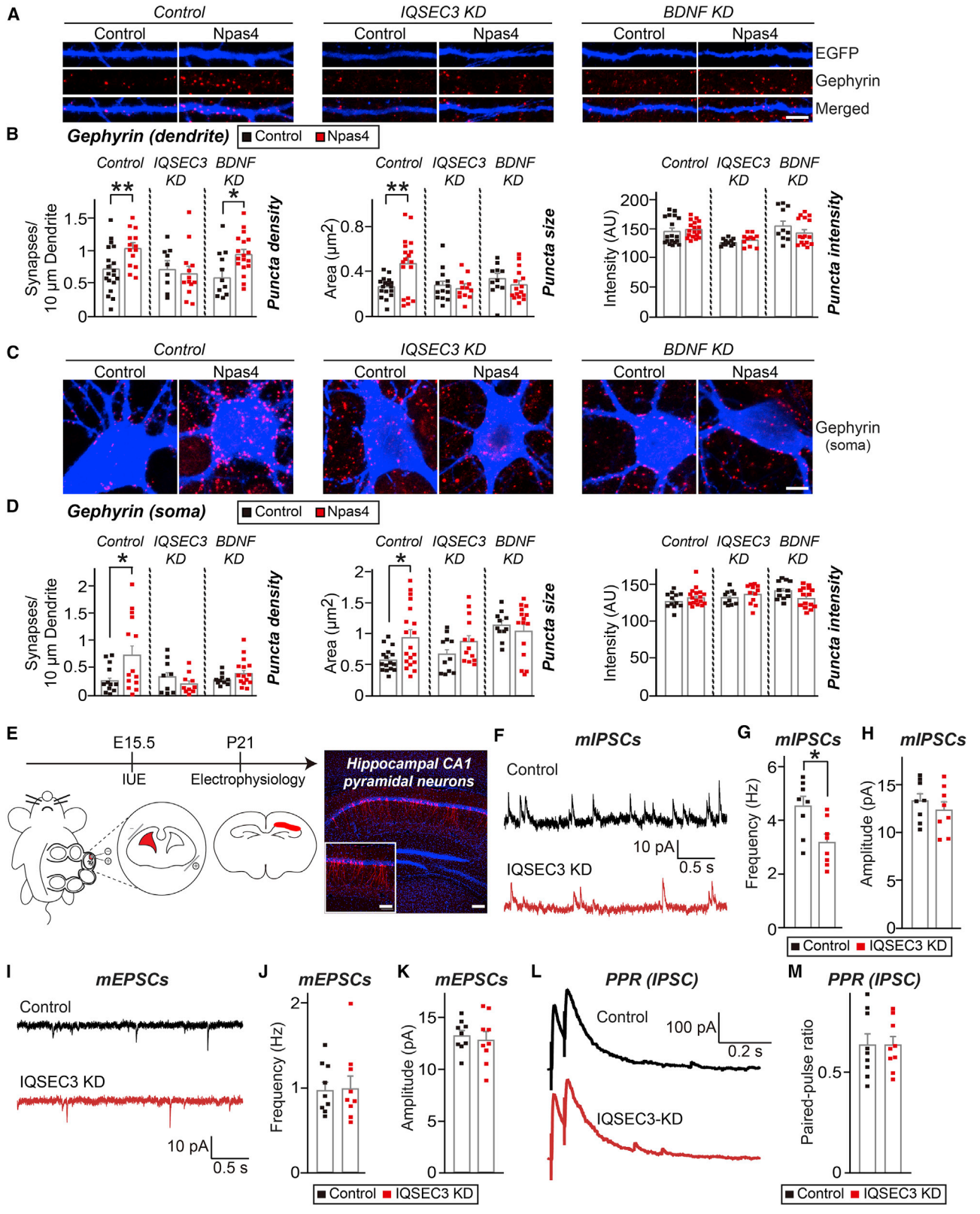

(legend on next page)

IQSEC3 expression is specifically upregulated in somatostatin-positive interneurons of the hippocampal CA1 region

It was previously reported that the expression of *Npas4* and *Bdnf* mRNAs changes in response to neuronal depolarization (Bloodgood et al., 2013; Lin et al., 2008). Thus, we asked whether *Iqsec3* expression is also responsive to changes in neuronal activity. To test this, we used activity-altering protocols similar to those used to induce Npas4 expression, namely treatment with KA and exposure to an enriched environment (EE) (Bloodgood et al., 2013). We performed immunohistochemistry using ~11-week-old adult mice that were either injected with saline (SA) or 20 mg/kg KA (to induce neuronal hyperactivation) (Figure S1A). KA injections increased Npas4$^+$ cell numbers in both *stratum pyramidale* (SP) and *stratum oriens* (SO) layers of the hippocampal CA1 region, granule cell layer (GCL), and hilus of the DG (Figure S1A). Strikingly, KA injections resulted in an increase in the number of IQSEC3$^+$ cells and the proportion of IQSEC3$^+$ cells in neurons, specifically in the SO layer, but not in the SP layer, molecular layer, GCL, or hilus of the DG (Figures S1A and S1C). In addition, quantitative analyses using KA-injected Npas4$^{f/f}$ mice injected with adeno-associated viruses (AAVs) expressing Cre recombinase showed that Npas4 deletions decreased the number of IQSEC3$^+$ cells to a level that is comparable to that observed in SA-injected control mice in the SO layer (Figures S1B and S1C).

To further investigate the expression profile of IQSEC3 under physiological conditions in which network activity is heightened (avoiding pathological conditions, such as KA treatment), we manipulated the sensory experiences of juvenile wild-type (WT) mice by housing littermates in an EE, consisting of a running wheel and several novel objects that were regularly refreshed (Figure 3A). After 5 days in an EE setting, hippocampi were removed, sectioned, and immunostained for c-Fos as a surrogate measure of neuronal activity. As expected, EE exposure drove robust c-Fos expression in the hippocampal CA1 region (Figure 3B). We then performed immunohistochemical analyses on sections from age-matched mice housed in a standard environment (SE) as a control using previously validated antibodies recognizing Npas4 and IQSEC3 (Fukaya et al., 2011; Lin et al., 2008). Basal levels of Npas4 and IQSEC3 in the hippocampal CA1 region from mice housed under SE conditions were low (Figures 3C and 3D). Similar to KA-treated mice, there was a significant increase in the number of Npas4$^+$/IQSEC3$^+$ neurons in CA1 SO layers from mice allowed to explore an EE relative to those maintained in an SE (Figures 3C and 3D). Notably, IQSEC3 expression was also concomitantly increased in Npas4$^+$ neurons, an effect that was prominent in SO layers of the CA1 hippocampus (Figures 3C and 3D). EE-induced upregulation of IQSEC3 in the SO layer of the CA1 hippocampus was prominently observed in SST, but not parvalbumin (PV) or cholecystokinin (CCK), GABAergic interneurons (Figures 3E–3J). In addition, IQSEC3 was selectively upregulated in SST$^+$ GABAergic interneurons in the SO layer of the CA1 hippocampus of KA-treated mice (Figures S1D–S1I). These data show that IQSEC3 levels are preferentially altered specifically in SST$^+$ interneurons following the induction of neuronal activity *in vivo*.

RNAscope-based *in situ* hybridization analyses also showed that EE induced significant increases in IQSEC3 mRNA expression in SST$^+$ interneurons of the SO layer of the hippocampal CA1 region (Figures S2A–S2C). In contrast, EE induced a comparable increase in Npas4 mRNA expression in both SST$^+$ interneurons and pyramidal neurons (Figures S2D–S2F), suggesting the operation of a specific transcriptional mechanism for IQSEC3 mRNAs selectively in SST$^+$ interneurons.

To determine whether an activity-dependent increase in Npas4 level is responsible for the selective upregulation of IQSEC3 in the SO layer of the hippocampal CA1 region, we expressed either Cre or ΔCre in Npas4$^{f/f}$ mice via AAV-mediated stereotactic injection, and housed the resulting mice in either SE or EE conditions (Figure 3K). Quantitative immunohistochemical analyses showed that EE induced a significant increase in the number of Npas4$^+$ or IQSEC3$^+$ neurons, and Npas4 deletion blunted this effect, reducing the number of IQSEC3$^+$ neurons to a level comparable to that observed in SE-housed *Npas4*-cKO mice (Figures 3L–3O). Note that Bloodgood et al. (2013) estimated that 1% of neurons in the entire hippocampal CA1 area were positive for Npas4, whereas our quantification results showed that ~40% of neurons in the SO layer of the hippocampal CA1 region were positive for Npas4. This blunting of the number of IQSEC3$^+$ neurons was also recapitulated by the specific deletion of Npas4 in SST$^+$ interneurons from Cre-driver SST-Cre mice (Taniguchi et al., 2011) crossed with Npas4$^{f/f}$ mice (SST-*Npas4*-KO; Figures 3P–3S). These results support the

Figure 2. IQSEC3 mediates GABAergic synapse development as an Npas4 target and is required for inhibitory synaptic transmission *in vivo*

(A and C) Representative images of cultured hippocampal neurons infected at DIV3 with lentiviruses expressing EGFP alone (control), IQSEC3 KD, or BDNF KD, and transfected at DIV10 with lentiviral constructs expressing EGFP alone (control) or cotransfected with EGFP and Npas4 (Npas4). Dendrites (A) or cell bodies (C) of transfected neurons were analyzed by double-immunofluorescence labeling for gephyrin (red) and EGFP (blue) at DIV14. Scale bar, 10 μm.

(B and D) Summary graphs of the effects of IQSEC3 KD or BDNF KD in Npas4-expressing neurons on gephyrin puncta density (left), gephyrin puncta size (center), and gephyrin puncta intensity (right). Dendrites (B) and cell bodies (D) were quantified separately. Data are presented as means ± SEMs (*$p < 0.05$; **$p < 0.01$).

(E) Neuronal precursors were transfected at E15.5 with IQSEC3 KD vectors by *in utero* electroporation. Coronal mouse brain sections were prepared at post-natal day 21. Numerous tdTomato$^+$ neurons were detected in the CA1 hippocampal region. Scale bar, 100 μm.

(F–H) Effect of IQSEC3 KD on inhibitory synaptic transmission in hippocampal CA1 pyramidal neurons. Representative traces (F) and summary graphs of the frequencies (G) and amplitudes (H) of mIPSCs in hippocampal CA1 pyramidal neurons transfected with control or IQSEC3 KD are shown. Data are presented as means ± SEMs (*$p < 0.05$).

(I–K) Effect of IQSEC3 KD on excitatory synaptic transmission in hippocampal CA1 pyramidal neurons. Representative traces (I) and summary graphs of the frequencies (J) and amplitudes (K) of mEPSCs in hippocampal CA1 pyramidal neurons transfected with control or IQSEC3 KD are shown. Data are presented as means ± SEMs.

(L and M) Effect of IQSEC3 KD on PPR (amplitude of the second IPSC divided by that of the first). Representative traces (L) and a summary graph (M) of PPR measured at 50-ms interstimulus intervals are shown. Data are presented as means ± SEMs.

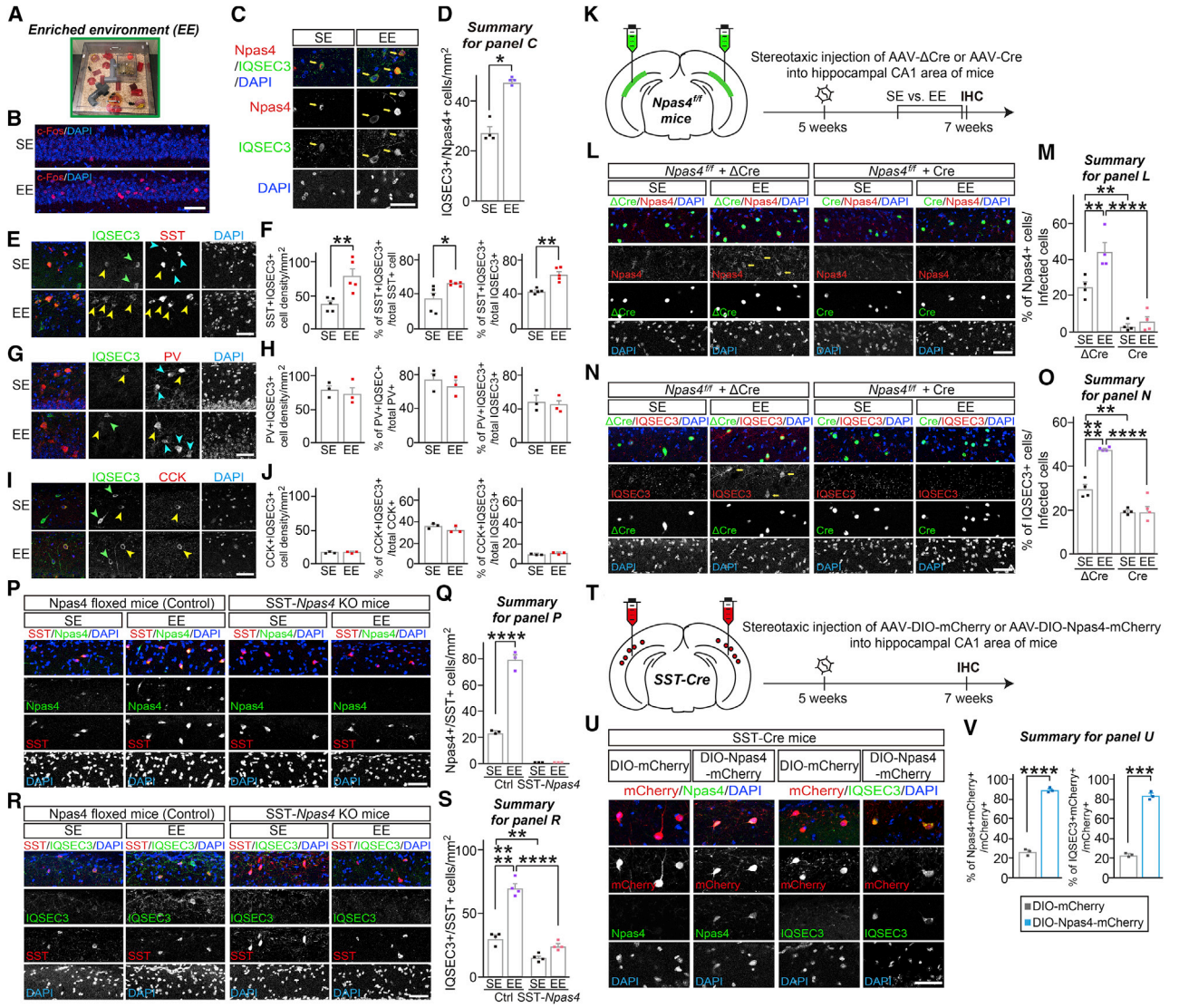

Figure 3. IQSEC3 protein level is regulated by neuronal activity and the presence of Npas4 *in vivo*

(A) The enriched environment (EE) setting, including tunnels, shelters, toys, and running wheels for voluntary exercise, used in the present study.

(B) Representative immunofluorescence images of hippocampal CA1 regions from adult (11-week-old) WT mice in a standard environment (SE) or EE setting were immunostained for c-Fos (red) and counterstained with DAPI (blue). Scale bar, 50 μm.

(C) Representative immunofluorescence images of the hippocampal CA1 SO layer from WT mice in an SE or EE setting were immunostained for Npas4 (red) and IQSEC3 (green), and counterstained with DAPI (blue). Note that yellow arrows indicate the interneurons with upregulated Npas4 or IQSEC3 levels in the SO layer. Scale bar, 50 μm.

(D) Bar graphs summarizing the density of IQSEC3/Npas4 double-positive neurons shown in (C). Data are presented as means ± SEMs (*$p < 0.05$).

(E, G, and I) Representative immunofluorescence images of the hippocampal CA1 SO layer from WT mice in an SE or EE setting, immunostained for IQSEC3 (green), DAPI (blue), and SST (red) (E), PV (red) (G), or CCK (red) (I). Yellow arrows mark cells coexpressing IQSEC3 and the indicated marker, cyan arrows mark cells expressing the indicated marker only, and green arrows mark cells expressing IQSEC3 only. Scale bar, 50 μm.

(F, H, and J) Bar graphs summarizing the quantitative results showing the density of IQSEC3$^+$ interneurons (left), the proportion of IQSEC3$^+$ interneurons (center), and the proportion of each IQSEC3$^+$ interneuron type (right) shown in (E), (G) and (I) in SST (F), PV (H), and CCK (J) interneurons. Data are presented as means ± SEMs (*$p < 0.05$; **$p < 0.01$).

(K) Experimental scheme for immunohistochemistry. The CA1 region of the hippocampus of ~5-week-old *Npas4*$^{f/f}$ mice was bilaterally injected with AAVs expressing ΔCre or Cre. Mice were housed for 5 days in an SE or EE setting 9 days after AAV injections and then analyzed by immunohistochemistry.

(L and N) Representative immunofluorescence images of the hippocampal CA1 SO layer from *Npas4*$^{f/f}$ mice was bilaterally injected with AAVs expressing ΔCre or Cre in an SE or EE setting, immunostained for Npas4 (red) (L) or IQSEC3 (red) (N) and DAPI (blue). Green fluorescence indicates neurons infected with AAV-Cre or AAV-ΔCre. Note that yellow arrows indicate the SST$^+$ interneurons with upregulated Npas4 (L) or IQSEC3 (N) levels. Scale bar, 50 μm.

(M and O) Bar graphs summarizing the percentage of Npas4$^+$ (M) or IQSEC3$^+$ (O) cells shown in (L) and (N). Data are presented as means ± SEMs (**$p < 0.01$; ****$p < 0.0001$).

(legend continued on next page)

idea that Npas4 is required for EE-induced upregulation of IQSEC3, specifically in SST$^+$ interneurons of the SO layer of the hippocampal CA1 region.

In addition, overexpressing Npas4 specifically in SST$^+$ interneurons by stereotaxic injections of double-floxed, inverted open reading frame (DIO), Cre-dependent AAV expressing Npas4 into the CA1 hippocampal region of SST-Cre mice was sufficient to significantly increase the expression of IQSEC3 protein (Figures 3T–3V), suggesting that Npas4 expression is both sufficient and required for the upregulation of the IQSEC3 level *in vivo*.

IQSEC3 is required for postsynaptic GABAergic synaptic transmission in SST-*Npas4*-KO interneurons

To determine whether Npas4-induced increases in IQSEC3 levels in SST$^+$ interneurons have an impact on postsynaptic GABAergic transmission, we exposed the control or SST-*Npas4*-KO mice to EE conditions to induce Npas4 protein expression, as previously described (Bloodgood et al., 2013; Hartzell et al., 2018). We crossed *Npas4*$^{f/+}$ mice with *Npas4*$^{f/+}$; SST-Cre mice to produce *Npas4*$^{f/f}$;SST-Cre and *Npas4*$^{+/+}$; SST-Cre mice as littermates and used them for various functional experiments (Figure 4A). We stereotactically injected AAV-DIO-mCherry alone (control), IQSEC3 WT (AAV-DIO-IQSEC3 WT), or the ARF-GEF-inactive IQSEC3 E749A mutant (AAV-DIO-IQSEC3 dominant-negative [DN]) into the hippocampal CA1 region of SST-*Npas4*-KO mice (Figure 4B). To assess changes in GABAergic synaptic currents, we obtained voltage-clamp recordings from mCherry fluorescent SST$^+$ interneurons. Recordings from SST$^+$ interneurons of the hippocampal CA1 region revealed significant reductions in the frequencies (but not amplitudes) of mIPSCs in SST-*Npas4*-KO mice (Figures 4C–4E). Remarkably, the restricted introduction of IQSEC3 WT, but not IQSEC3 DN, into SST-*Npas4*-KO mice rescued the deficits in GABAergic synaptic transmission (Figures 4C–4E). Notably, the overexpression of IQSEC3 WT in SST-Cre mice did not alter the frequency of mIPSCs, whereas the overexpression of IQSEC3 DN significantly decreased it (Figure S3). Parallel recordings from SST-*Npas4*-KO interneurons showed no changes in the frequencies or amplitudes of mEPSCs (Figures 4F–4H). These phenotypes in hippocampal CA1 SST$^+$ interneurons are different from a previous report that deletion of Npas4 decreased the frequency of mEPSCs in SST$^+$ interneurons of the visual cortex (Spiegel et al., 2014). Notably, the input resistance of SST-*Npas4*-KO interneurons was increased compared to that of control neurons (Table S2).

To corroborate these electrophysiological data, we performed semiquantitative immunohistochemical analyses of the same experimental groups in SST-*Npas4*-KO mice, and found that Npas4 deletion in SST$^+$ interneurons significantly reduced the punctate immunoreactivity of $GABA_AR\gamma2$ ($GABA_AR\gamma2$ subunit), vesicular GABA transporter (VGAT), and glutamate decarboxylase 67 (GAD67) within the mCherry$^+$ somata or dendrites of SST$^+$ interneurons in the SO layer of the hippocampus CA1 region (Figures 4I–4K). Again, selective expression of IQSEC3 WT, but not IQSEC3 DN, completely reversed the decreased density of the tested GABAergic synaptic marker proteins (Figures 4I–4K). We then determined whether IQSEC3 levels in SST$^+$ interneurons have an impact on the number of GABAergic synapses by injecting AAV-DIO-shIQSEC3 into the hippocampal CA1 of SST-Cre mice (Figure S4A). Semiquantitative immunohistochemical analyses showed that the overlap in the area of the punctate immunoreactivity of $GABA_AR\gamma2$ ($GABA_AR\gamma2$ subunit), VGAT, and GAD67 with the mCherry$^+$ somata or dendrites of SST$^+$ interneurons in the SO layer of the hippocampus CA1 region was markedly reduced in SST-specific IQSEC3 KD mice compared with that in control mice (Figures S4B–S4D). Remarkably, the transduction of SST interneurons with AAVs expressing DIO-IQSEC3 WT, but not those expressing DIO-IQSEC3 DN, completely reversed the decreased density of $GABA_AR\gamma2$ puncta (Figures S4B–S4D). These data suggest that IQSEC3 in SST$^+$ CA1 hippocampal neurons postsynaptically regulates Npas4-mediated activity-dependent GABAergic synaptic transmission *in vivo*.

The Npas4-IQSEC3 complex in SST$^+$ interneurons controls the neuronal activity of hippocampal CA1 pyramidal neurons

To further test whether the reduction in synaptic inhibition in CA1 SST$^+$ interneurons of SST-*Npas4*-KO mice alters neuronal activation in CA1 pyramidal neurons, we exposed control and SST-*Npas4*-KO mice to EE conditions for 5 days and then examined the activity of CA1 pyramidal neurons by immunohistochemically monitoring c-Fos expression (Figure 5A). We found that Npas4 deletion in SST$^+$ interneurons significantly decreased the number of c-Fos$^+$ cells in the CA1 SP layer (Figures 5B and 5C). Again, the expression of IQSEC3 WT, but not that of IQSEC3 DN, in SST-*Npas4*-KO interneurons normalized the altered c-Fos

(P) Representative immunofluorescence images of the hippocampal CA1 SO layer from control or SST-*Npas4* mice under SE or EE conditions, immunostained for Npas4 (green), SST (red), and DAPI (blue). Scale bar, 50 μm.

(Q) Bar graphs summarizing the number of Npas4$^+$ cells expressed in SST$^+$ interneurons shown in (P). Data are presented as means ± SEMs (****$p < 0.0001$).

(R) Representative immunofluorescence images of the hippocampal CA1 SO layer from control or SST-*Npas4*-KO mice under SE or EE conditions, immunostained for SST (red), IQSEC3 (green), and DAPI (blue). Scale bar, 50 μm.

(S) Bar graphs summarizing the number of IQSEC3$^+$ cells expressed in SST$^+$ interneurons shown in (R). Data are presented as means ± SEMs (**$p < 0.01$; ****$p < 0.0001$).

(T) Experimental scheme for immunohistochemistry. The CA1 region of the hippocampus of ~5-week-old SST-Cre mice was bilaterally injected with AAVs expressing Cre-dependent mCherry or Cre-dependent Npas4-mCherry. The injected mice were analyzed by immunohistochemistry 2 weeks after injection.

(U) Representative immunofluorescence images of the hippocampal CA1 SO layer from SST-Cre mice was bilaterally injected with AAVs expressing DIO-mCherry or DIO-Npads4-mCherry and immunostained for Npas4 (green) (left) or IQSEC3 (green) (right), and DAPI (blue). Red fluorescence indicates neurons infected with the indicated Cre-dependent AAVs. Scale bar, 50 μm.

(V) Bar graphs summarizing the proportion of Npas4$^+$ cells (left) and the proportion of IQSEC3$^+$ cells (right) expressed in SST$^+$ interneurons infected with AAV-DIO-mCherry or AAV-DIO-Npas4. Data are presented as means ± SEMs (***$p < 0.001$; ****$p < 0.0001$).

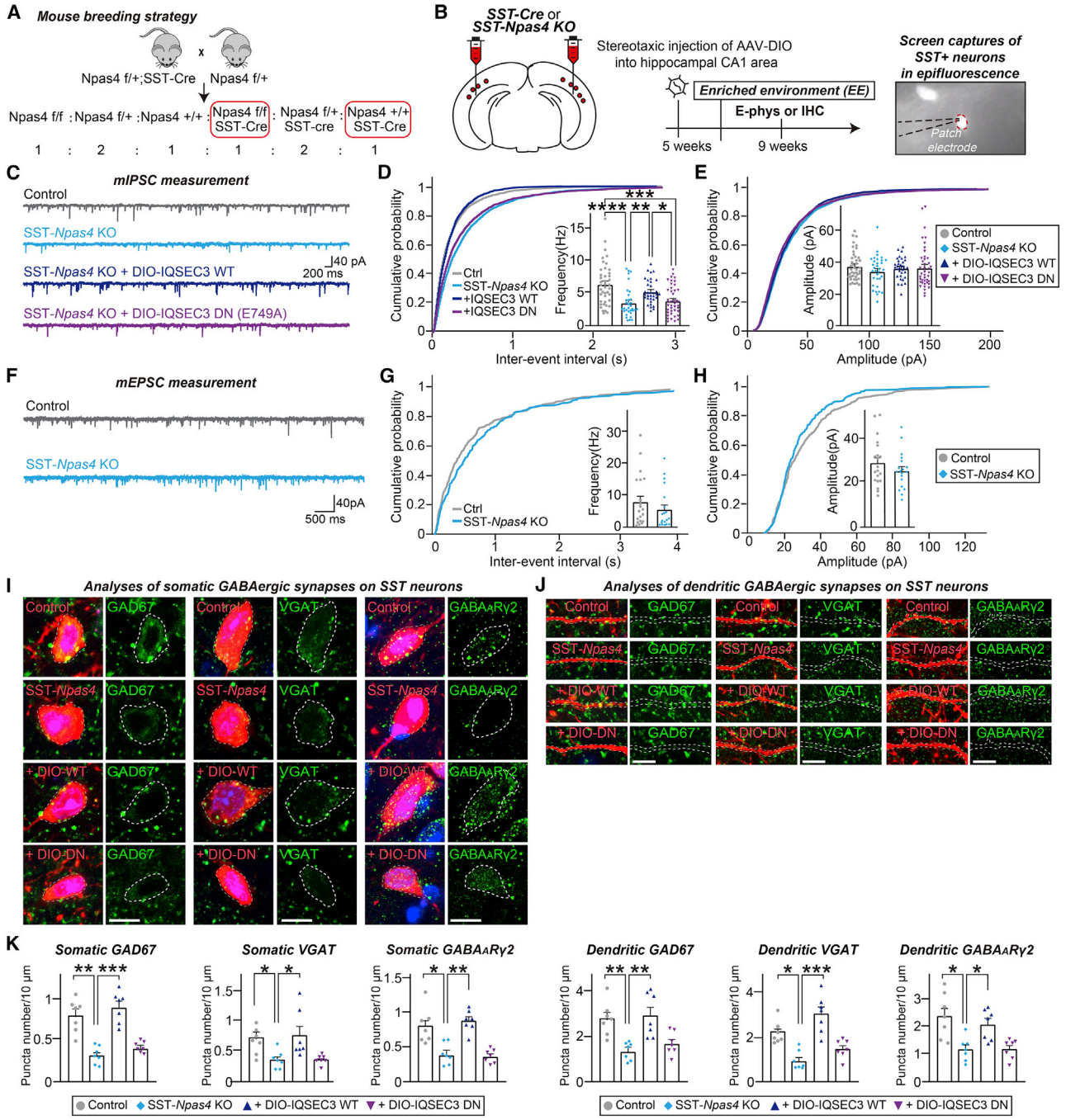

Figure 4. IQSEC3 functions as a downstream effector of Npas4 in regulation of GABAergic synaptic transmission in SST$^+$ interneurons

(A) Mouse breeding strategy for producing the SST-*Npas4* and littermate control mice used in functional experiments. Among the genotypes of offspring, the mice in the red boxes were used for experiments.

(B) Experimental configuration for *ex vivo* electrophysiology experiments (C–H).

(C–E) Representative mIPSC traces (C) and cumulative distribution of mIPSC frequencies (D) and amplitudes (E) in SST$^+$ interneurons from SST-*Npas4*-KO mice exposed to EE conditions. Insets show average mIPSC frequencies (D) and amplitudes (E). Data are presented as means ± SEMs (*p < 0.05; **p < 0.01; ***p < 0.001; ****p < 0.0001).

(legend continued on next page)

expression (Figures 5B and 5C). These observations suggest that Npas4 acts through IQSEC3 in SST$^+$ interneurons in a manner that depends on IQSEC3 ARF-GEF activity to dictate dendritic synaptic inhibition and activity in hippocampal pyramidal neurons *in vivo*.

IQSEC3 mediates hippocampal CA1 SST- and Npas4-dependent anxiety-like behavior

Lastly, we investigated the behavioral effects of IQSEC3 expression in Npas4-KO mice. Npas4-KO mice have been reported to exhibit diverse cognitive, emotional, and social behavioral deficits (Heroux et al., 2018; Shepard et al., 2017; Sun and Lin, 2016; Weng et al., 2018). Similar to the other histological or electrophysiological analyses, SST-*Npas4*-KO and littermate control mice were exposed to EE conditions for 5 days before performing a number of behavioral tasks, including elevated plus maze (EPM), novelty-suppressed feeding (NSF), light-dark transition (LDT), Y-maze, open-field (OF), novel object recognition (NOR), and forced swim (FS) tests, to determine whether hippocampal CA1 electrophysiological phenotypes in Npas4-KO mice are linked to behavioral abnormalities, and to assess the role of IQSEC3 in regulating Npas4-mediated behavior. SST-*Npas4*-KO mice were additionally injected in the hippocampal CA1 region with AAV-DIO-mCherry, AAV-DIO-IQSEC3 WT, or AAV-DIO-IQSEC3 DN (Figure 6A). SST-specific *Npas4*-KO mice exhibited reduced anxiety-like behavior, as evidenced by increased time spent in open arms (with a similar number of entries into each open arm) in the EPM test (Figures 6B–6D and S5A–S5C), increased time spent in the light compartment in the LDT test (Figures 6H and 6I), and decreased latency to feed in the NSF test (Figure 6J–6L), but showed normal depressive-related behavior (as assessed by FS; Figures S6A and S6B), normal locomotor activity (as assessed by the OF test; Figure S6C–S6F), normal working memory (as assessed by the Y-maze test; Figures S6G–S6I), and normal recognition memory (as assessed by the NOR test; Figures S6J–S6M)—phenotypes that are slightly different from those of constitutive Npas4-KO mice (Coutellier et al., 2012; Jaehne et al., 2015). Strikingly, expression of IQSEC3 WT in CA1 SST$^+$ interneurons was sufficient to rescue the reduced anxiety-like behavior (EPM, LDT, and NSF tests) observed in SST-specific *Npas4*-KO mice (Figures 6B–6D and 6H–6L). Intriguingly, the expression of IQSEC3 DN failed to normalize the reduced anxiety-like behavior, suggesting that the ARF-GEF activity of IQSEC3 is essential for mediating the ability to form a subset of Npas4- and CA1 SST-dependent mouse behaviors (Figures 6B–6D and 6H–6L). Importantly, neither IQSEC3 WT nor IQSEC3 749A altered the anxiety-like behavior of SST-Cre mice (control; Figures 6E–6G and S5D–S5F), ruling out IQSEC3 gain-of-function effects on EPM tests. In line with the idea that IQSEC3 acts downstream of Npas4 in mediating anxiety-like behavior, selective IQSEC3 KD in CA1 SST$^+$ interneurons similarly recapitulated reduced anxiety-like behavior in the EPM test (the injected SST-Cre mice were exposed to EE conditions before the EPM test; Figures 6M–6P and S5G–S5I).

To further link the consequences of altered Npas4-IQSEC3 inhibitory synaptic complex with deficits in the hippocampal CA1 SST-dependent anxiety-like behaviors observed in SST-*Npas4*-KO mice, we selectively manipulated the activities of hippocampal CA1 SST$^+$ interneurons using an intersectional genetic approach employing the expression of designer receptors exclusively activated by designer drugs (DREADDs) (Urban and Roth, 2015). Control and SST-*Npas4*-KO mice were injected with Cre-dependent DIO AAVs expressing inhibitory (hM4Di) DREADDs (AAV-DIO-hM4Di) or mCherry alone (AAV-DIO-mCherry) (Figure 7A). The designer ligand clozapine-N-oxide (CNO) or SA was then delivered via intraperitoneal injection (3 mg/kg) 30 min before beginning the behavioral experiments (Figure 7A). We validated the inhibition of DREADD receptors by CNO by measuring firing rates in SST$^+$ interneurons (Figure 7B). SST$^+$ interneurons expressing hM4Di exhibited a decreased firing rate after CNO application in brain slices (Figure 7B). Injection of AAV-DIO-hM4Di, followed by CNO administration, into SST$^+$ interneurons of SST-Cre mice did not affect time spent in open arms in the EPM tests (Figures 7C–7E), suggesting that the inhibition of baseline CA1 SST$^+$ interneuron activity per se does not alter anxiety-like behavior in mice. In contrast, the injection of AAV-DIO-hM4Di into SST-*Npas4*-KO mice, followed by CNO administration, rescued the reduced anxiety-like behavior observed in SST-*Npas4*-KO mice (Figures 7C–7E and S5J–S5L), suggesting that the inhibitory action of Npas4 in CA1 SST$^+$ interneurons is causally involved in Npas4-mediated regulation of anxiety-like behavior. In contrast, the injection of Cre-dependent DIO-AAVs expressing excitatory (hM3Dq) DREADDs (AAV-DIO-hM3Dq) into SST-Cre mice, as validated by measuring firing rates in SST$^+$ interneurons of SST-Cre mice (Figures 7F and 7G), did not alter their anxiety-like behavior, regardless of housing conditions (Figures 7I–7M and S5M–S5R), suggesting that a balanced level of inhibition in the hippocampal CA1 circuitry is crucial for the maintenance of anxiety-like behavior. This *in vivo* DREADD approach was validated by showing that the expression of the phosphorylated form of ERK1/2 (pERK), a downstream target of Gq-DREADD (Armbruster et al., 2007), in hM3Dq-expressing CA1 SST$^+$ neurons was induced only when CNO was applied (Figure 7H).

DISCUSSION

IQSEC3 is linked to Npas4-mediated post-transcriptional programs that orchestrate activity-dependent GABAergic synapse organization. Npas4, a well-known transcription factor and putative upstream regulator of IQSEC3 (Bloodgood et al., 2013; Sun

(F–H) Representative mEPSC traces (F) and cumulative distribution of mEPSC frequencies (G) and amplitudes (H) in SST$^+$ interneurons from SST-*Npas4*-KO mice exposed to EE conditions. Insets show average mEPSC frequencies (G) and amplitudes (H). Data are presented as means ± SEMs (Mann-Whitney *U* test). See Table S2 for intrinsic electrophysiological properties of SST$^+$ interneurons from control and SST-*Npas4*-KO mice.

(I–K) Representative images (I) and (J) and quantification (K) of somatic GAD67$^+$, GABA$_A$Rγ2$^+$, and VGAT$^+$ puncta (I), and dendritic GAD67$^+$, GABA$_A$Rγ2$^+$, and VGAT$^+$ puncta (J) in SST$^+$ interneurons from SST-*Npas4*-KO mice exposed to EE conditions. Data are presented as means ± SEMs (*p < 0.05; **p < 0.01; ***p < 0.001). Scale bar, 10 μm.

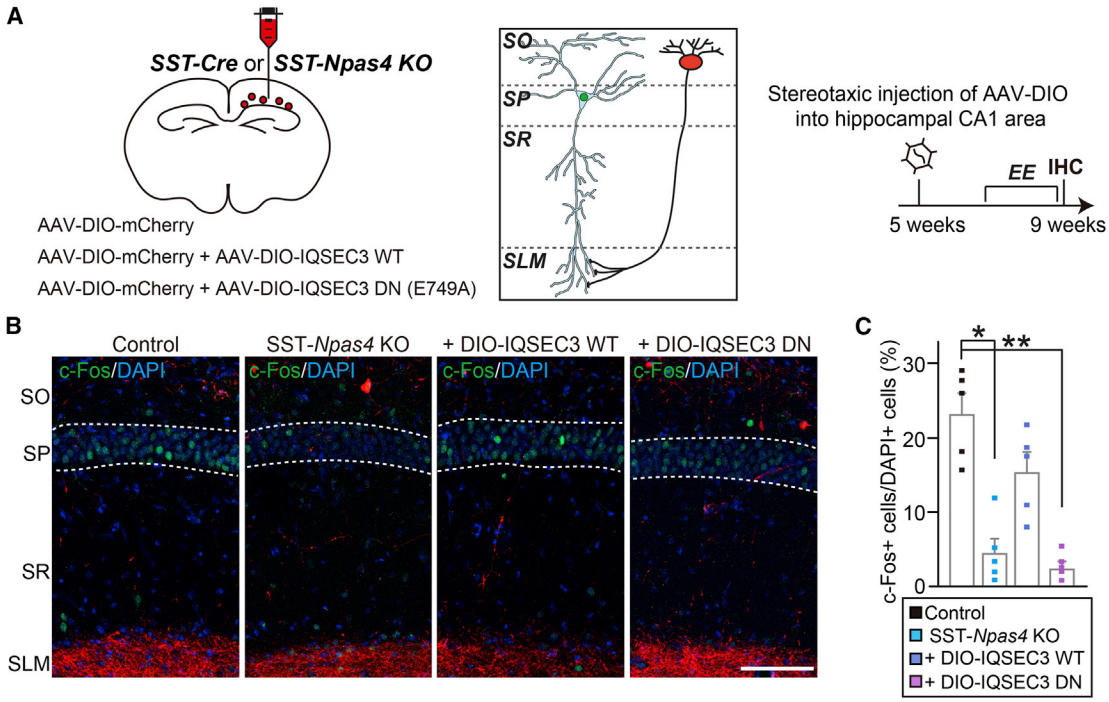

Figure 5. IQSEC3 expression in SST$^+$ interneurons determines activity of hippocampal CA1 pyramidal neurons

(A) Experimental configuration for immunohistochemistry experiments (B) and (C).

(B and C) Representative images (B) and quantification (C) of c-Fos puncta in hippocampal CA1 pyramidal neurons from SST-*Npas4*-KO mice exposed to EE conditions. Data are presented as means ± SEMs (*p < 0.05; **p < 0.01). Scale bar, 10 μm.

and Lin, 2016), binds to the promoter region of *Iqsec3*, which contains Npas4 consensus binding sites; IQSEC3 protein, in turn, functions downstream of Npas4 in regulating GABAergic inhibition in both somatic and dendritic compartments of cultured hippocampal neurons. IQSEC3 expression is specifically induced by the manipulation of synaptic activity *in vivo*, consistent with the idea that IQSEC3, whose corresponding gene is an Npas4 target, promotes activity-dependent GABAergic synapse organization. This interpretation is further supported by the observations that upregulated IQSEC3 protein levels in SST$^+$ interneurons of the hippocampal CA1 SO layer were completely compromised in SST-specific *Npas4*-KO mice. Although prior screens using GABAergic neuron-enriched cultures to profile activity-dependent transcriptomics and single-cell analyses in the mouse visual cortex failed to identify IQSEC3 as a stimulus-responsive gene (Hrvatin et al., 2018; Spiegel et al., 2014), experimental conditions used in these previous studies may have been unsuitable for identifying responsive genes that are specifically regulated in hippocampal CA1 SST$^+$ interneurons. In support of this, our results showed that Npas4 regulates inhibitory inputs onto SST$^+$ interneurons in the hippocampal CA1 region, contrary to a previous report that it specifically controls excitatory inputs onto SST$^+$ interneurons in the visual cortex (Spiegel et al., 2014). A similar precedent was documented in the cases of neuroligin-3 R451C knockin mice (Etherton et al., 2011; Tabuchi et al., 2007). Although more investigation is warranted, it is plausible that Npas4 uses different downstream targets across different brain areas—even in identical types of GABAergic interneurons with similar molecular profiles—to modulate input/output patterns of neuronal activation. Our results also suggest that context-dependent regulatory mechanisms may underlie Npas4-mediated transcriptional and post-transcriptional control of IQSEC3 levels *in vivo* (Tyssowski et al., 2018). Notably, Npas4 differentially dictates gene regulatory mechanisms tailored to the type of activity patterns along subcellular compartments of a neuron via the formation of distinct heterodimers with ARNT proteins (Brigidi et al., 2019). Whether these molecularly distinct induction mechanisms culminate in the formation of stimulus-specific Npas4 heterodimers in other neuron types, including SST$^+$ interneurons, should be clarified.

IQSEC3 performs the distinct actions as a Npas4 downstream component, compared to other known Npas4 targets that are involved in regulating neural circuit-wide homeostasis (BDNF and Homer1a), neuroprotective signaling (Syt-10), and synaptic plasticity during memory formation (Plk2) across various brain regions, neuron types, and synapse types (Shan et al., 2018; Spiegel et al., 2014; Weng et al., 2018; Woitecki et al., 2016). Loss of Npas4 function results in reduced GABAergic synapse density in both perisomatic and dendritic regions of cultured hippocampal neurons and blunts the inhibitory mode, concurrent with an abnormal distribution of GABAergic synapses at both soma and apical dendrites of CA1 pyramidal neurons (Lin et al., 2008; Bloodgood et al., 2013). BDNF is specifically upregulated by Npas4 overexpression in excitatory "cortical" neurons, and serves to specifically

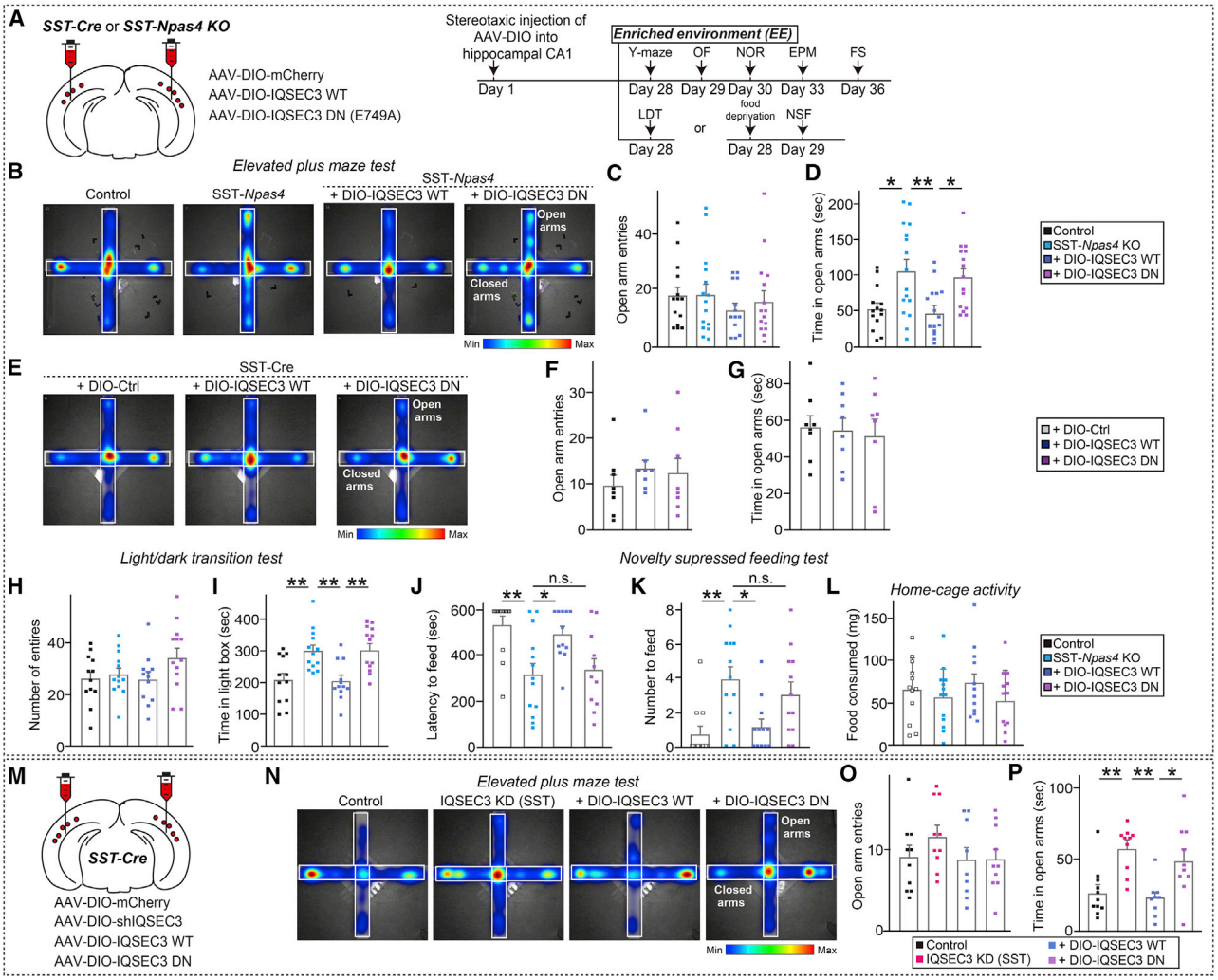

Figure 6. Expression of IQSEC3 WT, but not IQSEC3 E749A, in the hippocampal CA1 normalizes reduced anxiety-like behavior observed in SST-*Npas4*-KO mice

(A) Schematic diagram of mouse behavioral analyses. The CA1 region of the hippocampus of 5- to 6-week-old SST-*Npas4* mice was bilaterally injected with AAVs expressing mCherry (SST-*Npas4*-cKO), or either of two IQSEC3 DIO-AAVs (AAV-DIO-IQSEC3 WT or AAV-DIO-IQSEC3 DN [E749A]). SST-Cre mice injected with AAV-DIO-control-mCherry were used as controls. Injected mice were subjected to behavioral tasks 4 weeks after the injections in the indicated order. EPM, elevated plus-maze test; FS, forced swim test; LDT, light-dark transition test; NOR, novel object recognition test; NSF, novelty-suppressed feeding test; and OF, open-field test.

(B–D) Analysis of anxiety/exploration-related behavior by EPM test in SST-*Npas4*-KO injected with the indicated AAVs. Representative heatmaps of the time spent in the open arms of the EPM (B) are presented. Number of open arm entries (C) and time spent in open arms (D). Data are presented as means ± SEMs (*$p < 0.05$; **$p < 0.01$).

(E–G) Analysis of anxiety/exploration-related behavior by EPM test in SST-Cre injected with the indicated AAVs. Representative heatmaps of the time spent in the open arms of the EPM (E) are presented. Number of open arm entries (F) and time spent in open arms (G). Data are presented as means ± SEMs.

(H and I) Analysis of anxiety/exploration-related behavior by LDT test in SST-*Npas4*-KO mice injected with the indicated AAVs. Number of entries into the light chamber (H) and time spent in light chamber (I). Data are presented as means ± SEMs (**$p < 0.01$).

(J–L) Analysis of anxiety-related behavior by NSF test in SST-Cre injected with the indicated AAVs. Latency to feed (J), number to feed (K), and the amount of food consumed in the homecage (L) are presented. Data are presented as means ± SEMs (*$p < 0.05$; **$p < 0.01$).

(M) Schematic depiction of the experimental paradigm for IQSEC3 knockdown of hippocampal SST^+ interneurons.

(N–P) Analysis of anxiety/exploration-related behavior by EPM test in SST-Cre mice injected with the indicated AAVs. Representative heatmaps of the time spent in the open arms of the EPM (N) are presented. Red represents increased time spent, and blue represents minimal time spent during the test. Number of open arm entries (O) and time spent in open arms (P). Data are presented as means ± SEMs (*$p < 0.05$; **$p < 0.01$).

promote their perisomatic inhibition, whereas Plk2 is strongly expressed in excitatory "hippocampal" CA3 pyramidal neurons that regulate thorny excrescence structures at mossy fiber-CA3 synapses (Spiegel et al., 2014; Weng et al., 2018). Anatomical analyses in the present study revealed that IQSEC3, as an Npas4 downstream target, contributes to the regulation of

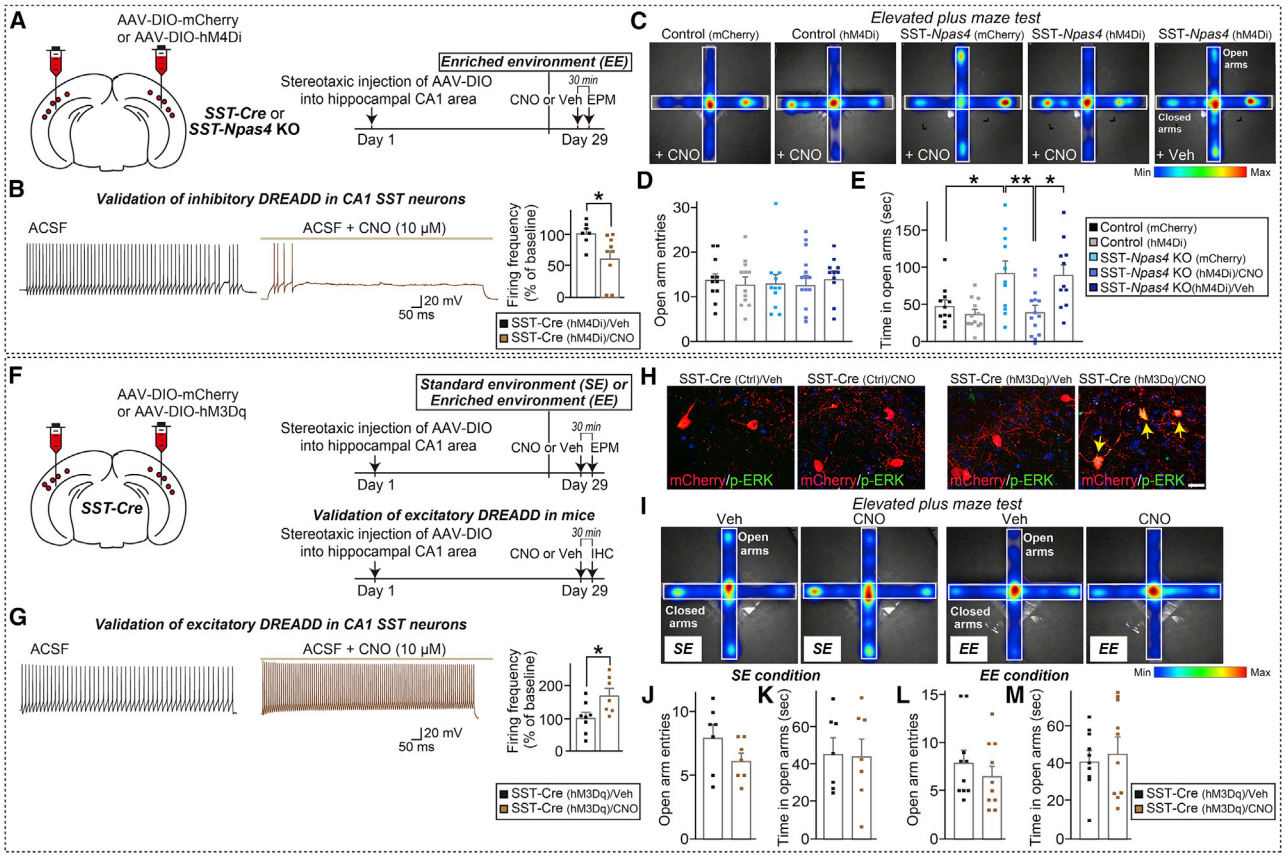

Figure 7. Inhibitory DREADD experiments demonstrate that inhibitory actions of Npas4 in hippocampal CA1 SST$^+$ interneurons regulate anxiety-like behavior

(A) Schematic depiction of the experimental paradigm for acute CNO-mediated DREADD inhibition of hippocampal SST$^+$ interneurons.

(B) Representative traces (left) and summary graphs (right) showing mean firing frequency (percentage) in hM4Di-mCherry expression induced by current injected before and during CNO (10 μM) treatment. Data are presented as means ± SEMs (*$p < 0.05$).

(C–E) Effects of acute CNO-mediated hM4Di inhibition of hippocampal CA1 SST$^+$ interneurons on anxiety/exploration-related behavior in control and SST-*Npas4*-KO mice, as measured by EPM test. All of the mice were housed under either EE condition. Representative heatmaps of the time spent in the open arms of the EPM (C) are presented. Red represents increased time spent and blue represents minimal time spent during the test. Number of open arm entries (D) and time spent in open arms (E) were measured. Additional measured parameters are presented in Figure S5. Data are presented as means ± SEMs (*$p < 0.05$; **$p < 0.01$).

(F) Schematic depiction of the experimental paradigm for acute CNO-mediated DREADD excitation of hippocampal SST$^+$ interneurons.

(G) Representative traces (left) and summary graphs (right) showing mean firing frequency (percentage) in hM3Dq-mCherry-expressing SST$^+$ neurons induced by current injected before and during CNO (10 μM) treatment. Data are presented as means ± SEMs (*$p < 0.05$).

(H) Histomolecular validation of hM3Dq in mice. Representative immunofluorescence images of hippocampal CA1 SST$^+$ interneurons from mice expressing hM3Dq-mCherry, intraperitoneally injected with either saline (Veh.) or CNO (3 mg/kg), and immunostained for mCherry (red) and pERK (green). Yellow arrows mark cells coexpressing mCherry and pERK. Scale bar, 20 μm.

(I–M) Effects of acute CNO-mediated hM3Dq excitation of hippocampal CA1 SST$^+$ interneurons on anxiety/exploration-related behavior in SST-Cre mice housed under SE or EE conditions, as measured by EPM test. Representative heatmaps of the time spent in the open arms of the EPM (I) are presented. Red represents increased time spent and blue represents minimal time spent during the test. Number of open arm entries (J) and (L) and time spent in open arms (K) and (M) were measured. Additional measured parameters are presented in Figure S5. Data are presented as means ± SEMs.

neural circuit properties in CA1 SST$^+$ interneurons, thereby further controlling the activity of CA1 pyramidal neurons.

This mechanism of IQSEC3 action is in stark contrast to the specific mode of action of BDNF and neuroligin-2 at perisomatic regions of hippocampal neurons (Bloodgood et al., 2013; Gibson et al., 2009; Lin et al., 2008). These observations may be integrated under a scenario in which altered inhibitory synapse organization in both somatic and dendritic compartments of IQSEC3-deficient neurons involves at least two distinct pathways *in vivo*. Consistent with this speculation, activity-dependent upregulation of IQSEC3 was notable in SST$^+$ interneurons (but not excitatory neurons) of the hippocampal CA1 region, suggesting that one plausible role of IQSEC3 in SST$^+$ interneurons is to increase inhibitory inputs onto them, enabling Npas4 to manage optimal responses and enhance feedback inhibition of principal neurons within local neural circuits in a context-dependent fashion. Notably, the overexpression of IQSEC3 E749A in CA1 SST$^+$ neurons did not alter the anxiety-like behavior,

whereas IQSEC3 KD in CA1 SST$^+$ neurons reduced anxiety-like behavior, despite both manipulations similarly reducing inhibitory synaptic transmission onto CA1 SST$^+$ neurons. Re-expression of IQSEC3 E749A in IQSEC3-deficient neurons failed to rescue the deficits in inhibitory synaptic transmission and abnormal anxiety-like behavior, suggesting that ARF GEF activity of IQSEC3 is critical for both inhibitory synaptic function and maintenance of anxiety-like behavior. However, other (un)identified functions of IQSEC3 that should be interdependent with its ARF GEF activity are also likely to be involved in mediating Npas4-mediated anxiety-like behavior, but not in regulating inhibitory synapse organization. Given that IQSEC3 is expressed in various types of interneurons as well as excitatory neurons in mouse hippocampal regions, it is likely that IQSEC3 differentially shapes specific circuit features that modulate homeostatic plasticity at distinct principal neuron-interneuron synapses. SST$^+$ interneurons also provide inhibitory input to PV$^+$ interneurons, which preferentially innervate the perisomatic region and axon initial segment of pyramidal cells, thereby controlling their spike output (Pelkey et al., 2017). Thus, the increased inhibition of PV$^+$ cells by disinhibited SST$^+$ interneurons may also contribute to the disinhibition of pyramidal cells in SST-*Npas4*-KO mice. Future studies in which Npas4 is conditionally deleted in PV$^+$ interneurons are warranted to clarify this issue.

The expression of IQSEC3 in CA1 SST$^+$ interneurons completely normalized the altered anxiety-like behavior of SST-specific *Npas4*-KO mice, suggesting that a distinct set of factors downstream of Npas4 is required for the modulation of a spectrum of hippocampus-dependent cognitive and behavioral tasks (Ramamoorthi et al., 2011; Weng et al., 2018). More importantly, our results suggest that the altered anxiety-like behavioral phenotype of SST-*Npas4*-KO mice reflects the differential GABAergic inhibition of pyramidal cells by the context-dependent, balanced activity of SST$^+$ interneurons and PV$^+$ interneurons. Conditional transgenic mice in which IQSEC3 is selectively deleted in specific interneurons should be further analyzed to address how various neural circuits involving different cell types are altered in the context of the synaptic functions of IQSEC3 proposed in the present study. This further study is especially meaningful given the implications of SST$^+$ interneurons in modulating anxiolytic brain states and major depressive disorders through the control of inhibition at specific synapse types formed in discrete neural circuits (Fee et al., 2017; Fuchs et al., 2017; Klausberger et al., 2003; Lin and Sibille, 2015). Other intriguing questions include whether the hyperexcitability of SST$^+$ interneurons leads to the increased expression and release of SST peptides that may contribute to the behavioral phenotype of SST-*Npas4*-KO mice, and how ARF6 signaling pathways dictated by IQSEC3 are differentially engaged in a cell-type-specific manner (Kim et al., 2020a). Further investigation is warranted to determine whether the upregulation of IQSEC3 triggered by Npas4 activation is observed in other regions of the brain or is specific to the hippocampal CA1 region, as documented in the present study.

In conclusion, our observations underscore the significance of biochemical complexes involving IQSEC3, Npas4, ARFs, and other components in organizing activity-dependent GABAergic synapse number and transmission and in shaping specific neural circuit architectures involved in anxiety-like behavior.

STAR★METHODS

Detailed methods are provided in the online version of this paper and include the following:

- KEY RESOURCES TABLE
- RESOURCE AVAILABILITY
  - Lead contact
  - Materials availability
  - Data and code availability
- EXPERIMENTAL MODEL AND SUBJECT DETAILS
  - Cell culture
  - Animals
- METHOD DETAILS
  - Construction of expression vectors
  - Antibodies
  - *Iqsec3* promoter-luciferase reporter analysis
  - Electrophoretic mobility shift assay
  - Chromatin immunoprecipitation assays
  - Chemicals
  - Neuron culture, transfections, imaging, and quantitation
  - Quantitative RT-PCR
  - AAV production, stereotactic surgery and virus injection
  - Activity alteration protocols
  - RNAscope assay
  - Immunohistochemistry and imaging
  - *In utero* electroporation
  - Electrophysiology
  - Mouse behavioral tests
  - Chemogenetic manipulation with DREADDs
- QUANTIFICATION AND STATISTICAL ANALYSIS
  - Data analysis and statistics

SUPPLEMENTAL INFORMATION

Supplemental information can be found online at https://doi.org/10.1016/j.celrep.2021.109417.

ACKNOWLEDGMENTS

We are grateful to Jinha Kim (DGIST) for technical assistance and to Drs. Yingxi Lin (MIT, USA), Michael Greenberg (Harvard University, USA), Minmin Luo (Tsinghua University, China), and Hiroyuki Sakagami (Kitasato University, Japan) for kindly providing published reagents. This study was supported by grants from the Brain Research Program through the NRF funded by the Ministry of Science and ICT & Future Planning (2017M3C7A1023470 to Jaewon Ko; 2017M3C7A1023471 to E.C.; and 2019R1A2C1086048 and 2020R1A4A1019009, to J.W.U.) and the DGIST R&D Program of the Ministry of Science and ICT (21-CoE-BT-01 to J.W.U. and Jaewon Ko).

AUTHOR CONTRIBUTIONS

J.W.U. and Jaewon Ko conceived and directed the project; S.K., D.P., Jinhu Kim, D.K., H.K., T.M., H.J., D.L., S.H., and J.J. performed the experiments; S.K., D.P., Jinhu Kim, T.M., K.T., E.C., Jaehoon Kim, J.W.U., and Jaewon

Ko analyzed the data; and J.W.U. and Jaewon Ko wrote the manuscript. All of the authors read and commented on the manuscript.

DECLARATION OF INTERESTS

The authors declare no competing interests.

Received: August 2, 2020
Revised: February 11, 2021
Accepted: June 28, 2021
Published: July 20, 2021

REFERENCES

Armbruster, B.N., Li, X., Pausch, M.H., Herlitze, S., and Roth, B.L. (2007). Evolving the lock to fit the key to create a family of G protein-coupled receptors potently activated by an inert ligand. Proc. Natl. Acad. Sci. USA *104*, 5163–5168.

Bloodgood, B.L., Sharma, N., Browne, H.A., Trepman, A.Z., and Greenberg, M.E. (2013). The activity-dependent transcription factor NPAS4 regulates domain-specific inhibition. Nature *503*, 121–125.

Brigidi, G.S., Hayes, M.G.B., Delos Santos, N.P., Hartzell, A.L., Texari, L., Lin, P.A., Bartlett, A., Ecker, J.R., Benner, C., Heinz, S., and Bloodgood, B.L. (2019). Genomic Decoding of Neuronal Depolarization by Stimulus-Specific NPAS4 Heterodimers. Cell *179*, 373–391.

Chen, L.F., Zhou, A.S., and West, A.E. (2017). Transcribing the connectome: roles for transcription factors and chromatin regulators in activity-dependent synapse development. J. Neurophysiol. *118*, 755–770.

Coutellier, L., Beraki, S., Ardestani, P.M., Saw, N.L., and Shamloo, M. (2012). Npas4: a neuronal transcription factor with a key role in social and cognitive functions relevant to developmental disorders. PLoS ONE *7*, e46604.

Etherton, M., Földy, C., Sharma, M., Tabuchi, K., Liu, X., Shamloo, M., Malenka, R.C., and Südhof, T.C. (2011). Autism-linked neuroligin-3 R451C mutation differentially alters hippocampal and cortical synaptic function. Proc. Natl. Acad. Sci. USA *108*, 13764–13769.

Fee, C., Banasr, M., and Sibille, E. (2017). Somatostatin-Positive Gamma-Aminobutyric Acid Interneuron Deficits in Depression: Cortical Microcircuit and Therapeutic Perspectives. Biol. Psychiatry *82*, 549–559.

Flores, C.E., and Méndez, P. (2014). Shaping inhibition: activity dependent structural plasticity of GABAergic synapses. Front. Cell. Neurosci. *8*, 327.

Fuchs, T., Jefferson, S.J., Hooper, A., Yee, P.H., Maguire, J., and Luscher, B. (2017). Disinhibition of somatostatin-positive GABAergic interneurons results in an anxiolytic and antidepressant-like brain state. Mol. Psychiatry *22*, 920–930.

Fukaya, M., Kamata, A., Hara, Y., Tamaki, H., Katsumata, O., Ito, N., Takeda, S., Hata, Y., Suzuki, T., Watanabe, M., et al. (2011). SynArfGEF is a guanine nucleotide exchange factor for Arf6 and localizes preferentially at post-synaptic specializations of inhibitory synapses. J. Neurochem. *116*, 1122–1137.

Gibson, J.R., Huber, K.M., and Südhof, T.C. (2009). Neuroligin-2 deletion selectively decreases inhibitory synaptic transmission originating from fast-spiking but not from somatostatin-positive interneurons. J. Neurosci. *29*, 13883–13897.

Hartzell, A.L., Martyniuk, K.M., Brigidi, G.S., Heinz, D.A., Djaja, N.A., Payne, A., and Bloodgood, B.L. (2018). NPAS4 recruits CCK basket cell synapses and enhances cannabinoid-sensitive inhibition in the mouse hippocampus. eLife *7*, e35927.

Heroux, N.A., Osborne, B.F., Miller, L.A., Kawan, M., Buban, K.N., Rosen, J.B., and Stanton, M.E. (2018). Differential expression of the immediate early genes c-Fos, Arc, Egr-1, and Npas4 during long-term memory formation in the context preexposure facilitation effect (CPFE). Neurobiol. Learn. Mem. *147*, 128–138.

Hrvatin, S., Hochbaum, D.R., Nagy, M.A., Cicconet, M., Robertson, K., Cheadle, L., Zilionis, R., Ratner, A., Borges-Monroy, R., Klein, A.M., et al. (2018). Single-cell analysis of experience-dependent transcriptomic states in the mouse visual cortex. Nat. Neurosci. *21*, 120–129.

Jaehne, E.J., Klarić, T.S., Koblar, S.A., Baune, B.T., and Lewis, M.D. (2015). Effects of Npas4 deficiency on anxiety, depression-like, cognition and sociability behaviour. Behav. Brain Res. *281*, 276–282.

Katz, L.C., and Shatz, C.J. (1996). Synaptic activity and the construction of cortical circuits. Science *274*, 1133–1138.

Kim, J., Guermah, M., McGinty, R.K., Lee, J.S., Tang, Z., Milne, T.A., Shilatifard, A., Muir, T.W., and Roeder, R.G. (2009). RAD6-Mediated transcription-coupled H2B ubiquitylation directly stimulates H3K4 methylation in human cells. Cell *137*, 459–471.

Kim, T.K., Hemberg, M., Gray, J.M., Costa, A.M., Bear, D.M., Wu, J., Harmin, D.A., Laptewicz, M., Barbara-Haley, K., Kuersten, S., et al. (2010). Widespread transcription at neuronal activity-regulated enhancers. Nature *465*, 182–187.

Kim, S., Kim, H., and Um, J.W. (2018). Synapse development organized by neuronal activity-regulated immediate-early genes. Exp. Mol. Med. *50*, 1–7.

Kim, H., Jung, H., Jung, H., Kwon, S.K., Ko, J., and Um, J.W. (2020a). The small GTPase ARF6 regulates GABAergic synapse development. Mol. Brain *13*, 2.

Kim, S., Kim, H., Park, D., Kim, J., Hong, J., Kim, J.S., Jung, H., Kim, D., Cheong, E., Ko, J., and Um, J.W. (2020b). Loss of IQSEC3 Disrupts GABAergic Synapse Maintenance and Decreases Somatostatin Expression in the Hippocampus. Cell Rep. *30*, 1995–2005.

Klausberger, T., Magill, P.J., Márton, L.F., Roberts, J.D., Cobden, P.M., Buzsáki, G., and Somogyi, P. (2003). Brain-state- and cell-type-specific firing of hippocampal interneurons in vivo. Nature *421*, 844–848.

Ko, J., Choii, G., and Um, J.W. (2015). The balancing act of GABAergic synapse organizers. Trends Mol. Med. *21*, 256–268.

Lin, L.C., and Sibille, E. (2015). Somatostatin, neuronal vulnerability and behavioral emotionality. Mol. Psychiatry *20*, 377–387.

Ko, J., Soler-Llavina, G.J., Fuccillo, M.V., Malenka, R.C., and Südhof, T.C. (2011). Neuroligins/LRRTMs prevent activity- and Ca^{2+}/calmodulin-dependent synapse elimination in cultured neurons. J. Cell Biol. *194*, 323–334.

Li, Y., Zeng, J., Zhang, J., Yue, C., Zhong, W., Liu, Z., Feng, Q., and Luo, M. (2018). Hypothalamic Circuits for Predation and Evasion. Neuron *97*, 911–924.

Lin, Y., Bloodgood, B.L., Hauser, J.L., Lapan, A.D., Koon, A.C., Kim, T.K., Hu, L.S., Malik, A.N., and Greenberg, M.E. (2008). Activity-dependent regulation of inhibitory synapse development by Npas4. Nature *455*, 1198–1204.

Mann, E.O., and Paulsen, O. (2007). Role of GABAergic inhibition in hippocampal network oscillations. Trends Neurosci. *30*, 343–349.

Martinelli, D.C., Chew, K.S., Rohlmann, A., Lum, M.Y., Ressl, S., Hattar, S., Brunger, A.T., Missler, M., and Südhof, T.C. (2016). Expression of C1ql3 in Discrete Neuronal Populations Controls Efferent Synapse Numbers and Diverse Behaviors. Neuron *91*, 1034–1051.

Oh, W.C., and Smith, K.R. (2019). Activity-dependent development of GABAergic synapses. Brain Res. *1707*, 18–26.

Park, D., Kim, S., Kim, H., Shin, J., Jung, H., and Um, J.W. (2020). Seizure progression triggered by IQSEC3 loss is mitigated by reducing activated microglia in mice. Glia *68*, 2661–2673.

Pelkey, K.A., Chittajallu, R., Craig, M.T., Tricoire, L., Wester, J.C., and McBain, C.J. (2017). Hippocampal GABAergic Inhibitory Interneurons. Physiol. Rev. *97*, 1619–1747.

Ploski, J.E., Monsey, M.S., Nguyen, T., DiLeone, R.J., and Schafe, G.E. (2011). The neuronal PAS domain protein 4 (Npas4) is required for new and reactivated fear memories. PLoS ONE *6*, e23760.

Ramamoorthi, K., Fropf, R., Belfort, G.M., Fitzmaurice, H.L., McKinney, R.M., Neve, R.L., Otto, T., and Lin, Y. (2011). Npas4 regulates a transcriptional program in CA3 required for contextual memory formation. Science *334*, 1669–1675.

Sakagami, H., Katsumata, O., Hara, Y., Tamaki, H., Watanabe, M., Harvey, R.J., and Fukaya, M. (2013). Distinct synaptic localization patterns of brefeldin A-resistant guanine nucleotide exchange factors BRAG2 and BRAG3 in the mouse retina. J. Comp. Neurol. *521*, 860–876.

Shamloo, M., Soriano, L., von Schack, D., Rickhag, M., Chin, D.J., Gonzalez-Zulueta, M., Gido, G., Urfer, R., Wieloch, T., and Nikolich, K. (2006). Npas4, a novel helix-loop-helix PAS domain protein, is regulated in response to cerebral ischemia. Eur. J. Neurosci. *24*, 2705–2720.

Shan, W., Nagai, T., Tanaka, M., Itoh, N., Furukawa-Hibi, Y., Nabeshima, T., Sokabe, M., and Yamada, K. (2018). Neuronal PAS domain protein 4 (Npas4) controls neuronal homeostasis in pentylenetetrazole-induced epilepsy through the induction of Homer1a. J. Neurochem. *145*, 19–33.

Sharma, N., Pollina, E.A., Nagy, M.A., Yap, E.L., DiBiase, F.A., Hrvatin, S., Hu, L., Lin, C., and Greenberg, M.E. (2019). ARNT2 Tunes Activity-Dependent Gene Expression through NCoR2-Mediated Repression and NPAS4-Mediated Activation. Neuron *102*, 390–406.

Shepard, R., Heslin, K., and Coutellier, L. (2017). The transcription factor Npas4 contributes to adolescent development of prefrontal inhibitory circuits, and to cognitive and emotional functions: implications for neuropsychiatric disorders. Neurobiol. Dis. *99*, 36–46.

Sim, S., Antolin, S., Lin, C.W., Lin, Y., and Lois, C. (2013). Increased cell-intrinsic excitability induces synaptic changes in new neurons in the adult dentate gyrus that require Npas4. J. Neurosci. *33*, 7928–7940.

Spiegel, I., Mardinly, A.R., Gabel, H.W., Bazinet, J.E., Couch, C.H., Tzeng, C.P., Harmin, D.A., and Greenberg, M.E. (2014). Npas4 regulates excitatory-inhibitory balance within neural circuits through cell-type-specific gene programs. Cell *157*, 1216–1229.

Sun, X., and Lin, Y. (2016). Npas4: Linking Neuronal Activity to Memory. Trends Neurosci. *39*, 264–275.

Sztainberg, Y., and Chen, A. (2010). An environmental enrichment model for mice. Nat. Protoc. *5*, 1535–1539.

Tabuchi, K., Blundell, J., Etherton, M.R., Hammer, R.E., Liu, X., Powell, C.M., and Südhof, T.C. (2007). A neuroligin-3 mutation implicated in autism increases inhibitory synaptic transmission in mice. Science *318*, 71–76.

Taniguchi, H., He, M., Wu, P., Kim, S., Paik, R., Sugino, K., Kvitsiani, D., Fu, Y., Lu, J., Lin, Y., et al. (2011). A resource of Cre driver lines for genetic targeting of GABAergic neurons in cerebral cortex. Neuron *71*, 995–1013.

Tyssowski, K.M., DeStefino, N.R., Cho, J.H., Dunn, C.J., Poston, R.G., Carty, C.E., Jones, R.D., Chang, S.M., Romeo, P., Wurzelmann, M.K., et al. (2018). Different Neuronal Activity Patterns Induce Different Gene Expression Programs. Neuron *98*, 530–546.

Um, J.W. (2017). Synaptic functions of the IQSEC family of ADP-ribosylation factor guanine nucleotide exchange factors. Neurosci. Res. *116*, 54–59.

Um, J.W., Choii, G., Park, D., Kim, D., Jeon, S., Kang, H., Mori, T., Papadopoulos, T., Yoo, T., Lee, Y., et al. (2016). IQ motif and SEC7 domain-containing protein 3 (IQSEC3) interacts with gephyrin to promote inhibitory synapse formation. J. Biol. Chem. *291*, 10119–10130.

Um, J.W., Han, K.A., Choi, S.Y., and Ko, J. (2020). Protocol for Quantitative Analysis of Synaptic Vesicle Clustering in Axons of Cultured Neurons. STAR Protoc *1*, 100095.

Um, J.W., Pramanik, G., Ko, J.S., Song, M.Y., Lee, D., Kim, H., Park, K.S., Südhof, T.C., Tabuchi, K., and Ko, J. (2014). Calsyntenins Function as Synaptogenic Adhesion Molecules in Concert with Neurexins. Cell Rep. *6*, 1096–1109.

Urban, D.J., and Roth, B.L. (2015). DREADDs (designer receptors exclusively activated by designer drugs): chemogenetic tools with therapeutic utility. Annu. Rev. Pharmacol. Toxicol. *55*, 399–417.

Weng, F.J., Garcia, R.I., Lutzu, S., Alviña, K., Zhang, Y., Dushko, M., Ku, T., Zemoura, K., Rich, D., Garcia-Dominguez, D., et al. (2018). Npas4 Is a Critical Regulator of Learning-Induced Plasticity at Mossy Fiber-CA3 Synapses during Contextual Memory Formation. Neuron *97*, 1137–1152.

West, A.E., and Greenberg, M.E. (2011). Neuronal activity-regulated gene transcription in synapse development and cognitive function. Cold Spring Harb. Perspect. Biol. *3*, a005744.

Woitecki, A.M., Müller, J.A., van Loo, K.M., Sowade, R.F., Becker, A.J., and Schoch, S. (2016). Identification of Synaptotagmin 10 as Effector of NPAS4-Mediated Protection from Excitotoxic Neurodegeneration. J. Neurosci. *36*, 2561–2570.

Wong, R.O., and Ghosh, A. (2002). Activity-dependent regulation of dendritic growth and patterning. Nat. Rev. Neurosci. *3*, 803–812.

Xu, W., and Südhof, T.C. (2013). A neural circuit for memory specificity and generalization. Science *339*, 1290–1295.

Yoshihara, S., Takahashi, H., Nishimura, N., Kinoshita, M., Asahina, R., Kitsuki, M., Tatsumi, K., Furukawa-Hibi, Y., Hirai, H., Nagai, T., et al. (2014). Npas4 regulates Mdm2 and thus Dcx in experience-dependent dendritic spine development of newborn olfactory bulb interneurons. Cell Rep. *8*, 843–857.

Yun, J., Nagai, T., Furukawa-Hibi, Y., Kuroda, K., Kaibuchi, K., Greenberg, M.E., and Yamada, K. (2013). Neuronal Per Arnt Sim (PAS) domain protein 4 (NPAS4) regulates neurite outgrowth and phosphorylation of synapsin I. J. Biol. Chem. *288*, 2655–2664.

STAR★METHODS

KEY RESOURCES TABLE

REAGENT or RESOURCE	SOURCE	IDENTIFIER
Antibodies		
Rabbit polyclonal anti-IQSEC3	Um et al., 2016	JK079; RRID: AB_2687864
Guinea pig anti-IQSEC3/SynArfGEF	Fukaya et al., 2011	Clone #: N6; RRID: AB_2314018
Rabbit polyclonal anti-Npas4	Bloodgood et al., 2013	RRID: AB_2687869
Mouse monoclonal anti-Npas4	NeuroMab	Cat #: 73-396; RRID: AB_2336900
Mouse monoclonal anti-GAD67	Millipore	Cat #: MAB5406; RRID: AB_2278725
Mouse monoclonal anti-Gephyrin	Synaptic Systems	Cat #: 147 011; RRID: AB_887717
Mouse monoclonal anti-PV	Swant	Cat #: PV 235; RRID: AB_10000343
Mouse monoclonal anti-SST	Millipore	Cat #: MAB354; RRID: AB_2255365
Rabbit polyclonal anti-CCK	ImmunoStar	Cat #: 20078; RRID: AB_572224
Goat polyclonal anti-EGFP	Rockland	Cat #: 600-101-215; RRID: AB_218182
Rabbit polyclonal anti-pERK1/2	Cell Signaling Technology	Cat #: 4370; RRID: AB_2315112
Cy3-conjugated donkey anti-rabbit	Jackson ImmunoResearch Laboratories	Cat #: 711-165-152; RRID: AB_2307443
Cy3-conjugated donkey anti-mouse	Jackson ImmunoResearch Laboratories	Cat #: 706-165-150; RRID: AB_2687868
Cy3-conjugated donkey santi-guinea pig	Jackson ImmunoResearch Laboratories	Cat #: 706-165-148; RRID: AB_2340460
FITC-conjugated donkey anti-mouse	Jackson ImmunoResearch Laboratories	Cat #: 715-035-150; RRID: AB_2340770
FITC-conjugated donkey anti-rabbit	Jackson ImmunoResearch Laboratories	Cat #: 711-095-152; RRID: AB_2315776
Chemicals, peptides, and recombinant proteins		
Pentobarbital sodium	Sigma	Cat #: P3761
Lipofectamine LTX Reagent with PLUS™ Reagent	ThermoFisher Scientific	Cat #: 15338100
Neurobasal medium	ThermoFisher Scientific	Cat #: 21103049
B-27 supplement (50X)	ThermoFisher Scientific	Cat #: 17504-044
Penicillin/Streptomycin	ThermoFisher Scientific	Cat #: 15140122
HBSS (Hanks' Balanced Salt Solution)	ThermoFisher	Cat #: 14065056
GlutaMax Supplement	ThermoFisher Scientific	Cat #: 35050061
Fetal Bovine Serum (FBS)	WELGENE	Cat #: PK004-01
Sodium pyruvate	ThermoFisher Scientific	Cat #: 11360070
Poly-D-lysine hydrobromide	Sigma	Cat #: P0899
DL-2-amino-5-phosphonopentanoic acid (DL-APV)	Abcam	Cat #: ab120003
DL-2-amino-5-phosphonopentanoic acid (DL-APV)	Sigma	Cat #: A5282
6-cyano-7-nitroquinoxaline-2,3-dione (CNQX)	Sigma	Cat #: C127
6,7-dinitroquinoxaline-2,3-dione (DNQX)	Abcam	Cat#: ab120018
Picrotoxin	Tocris	Cat #: 1128
Tetrodotoxin (TTX)	Tocris	Cat #: 1069
Potassium chloride (KCl)	ThermoFisher Scientific	Cat #: 7447-40-7
Polyethylene glycol (PEG)	Sigma	Cat #: P5413
Ethanol	Millipore	Cat #: 1.00983.1011
2,2,2-Tribromoethanol (Avertin)	Sigma	Cat #: T48402
Tert-amylalcohol (Avertin)	Sigma	Cat #: 24048-6
Vectashield mounting medium	Vector Laboratories	Cat #: H-1200
Clozapine N-oxide (CNO)	Tocris	Cat #: 4936
Critical commercial assays		
Sulfolink® Immobilization Kit for Proteins	ThermoFisher Scientific	Cat #: 44995
CalPhos Transfection Kit	Takara	Cat #: 631312

(*Continued on next page*)

Continued

REAGENT or RESOURCE	SOURCE	IDENTIFIER
Probe-Mm-*Iqsec3*-tv1	ACDBio	Cat #: 434961
Probe-Mm-*Iqsec3*-C2	ACDBio	Cat #: 434951-C2
Probe-Mm-*Npas4*-C2	ACDBio	Cat #: 423431-C2
Probe-Mm-*Sst*-C3	ACDBio	Cat #: 404631-C3
Experimental models: Cell lines		
HEK293T cells	ATCC	Cat #: CRL-3216
Cultured neuronal cells	N/A	N/A
Experimental models: Organisms/strains		
Mouse: C57BL/6N	The Jackson Laboratory	Cat #: 005304
Mouse: Npas4$^{f/f}$	Bloodgood et al., 2013	RRID: MGI: 3828102
Mouse: *Sst-ires*-Cre	The Jackson Laboratory	Cat #: 013044
Recombinant DNA		
L-315 shIQSEC3	Um et al., 2016	N/A
L-315 shBDNF	This paper	N/A
L-315 shNpas4	This paper	N/A
FSW-Cre-EGFP	Ko et al., 2011	N/A
FSW-ΔCre-EGFP	Ko et al., 2011	N/A
pcDNA3.1 Myc-Npas4	Lin et al., 2008	N/A
pAAV$_{2/9}$-Cre-IRES-EGFP	Xu and Südhof, 2013	N/A
pAAV$_{2/9}$-ΔCre-IRES-EGFP	Xu and Südhof, 2013	N/A
pAAV$_{2/9}$-Cre-IRES-tdTomato	Martinelli et al., 2016	N/A
pAAV$_{2/9}$-ΔCre-IRES-tdTomato	Martinelli et al., 2016	N/A
pAAV$_{2/9}$-DIO-Npas4-mCherry	This paper	N/A
pAAV$_{2/9}$-DIO-shIQSEC3-mCherry	This paper	N/A
pAAV$_{2/9}$-DIO-IQSEC3 WT	This paper	N/A
pAAV$_{2/9}$-DIO-IQSEC3 E749A (DN)	This paper	N/A
pAAV$_{8}$-DIO-mCherry	Addgene	Cat #: 50459
pAAV$_{8}$-DIO-hM3Dq-2A-mCherry	Li et al., 2018	N/A
pAAV$_{8}$-DIO-hM4Di-2A-mCherry	Addgene	Cat #: 50475
Software and algorithms		
MetaMorph	Molecular Devices	https://www.moleculardevices.com/
ImageJ	NIH	https://imagej.nih.gov/ij/
GraphPad Prism 7.0	GraphPad	https://www.graphpad.com
Mini Analysis	Synaptosoft	http://www.synaptosoft.com/MiniAnalysis
EthoVision XT 10.5	Noldus	https://www.noldus.com/animal-behavior-research/products/ethovision-xt
Statistical Package for the Social Sciences 23 (SPSS 23)	IBM	https://www.ibm.com

RESOURCE AVAILABILITY

Lead contact

Further information and requests for resources and reagents should be directed to and will be fulfilled by the Lead Contact, Dr. Ji Won Um (jiwonum@dgist.ac.kr).

Materials availability

All unique reagents generated in this study are available from the Lead Contact with a completed Materials Transfer Agreement.

Data and code availability

- All data supporting the findings of this study are available within the paper and are available from the Lead Contract upon request.

- This paper does not report original code.
- Any additional information required to reanalyze the data reported in this paper is available from the Lead Contact upon request.

EXPERIMENTAL MODEL AND SUBJECT DETAILS

Cell culture

HEK293T cells were cultured in Dulbecco's Modified Eagle's Medium (DMEM; WELGENE) supplemented with 10% fetal bovine serum (FBS; Tissue Culture Biologicals) and 1% penicillin-streptomycin (Thermo Fisher) at 37°C in a humidified 5% CO_2 atmosphere. Cultured primary hippocampal neurons were prepared from embryonic day 18 (E18) Sprague-Dawley rat brains (KOATECK). Neurons were seeded on 25-mm poly-D-lysine (0.1 mg/ml)–coated coverslips and cultured in Neurobasal media (GIBCO) containing penicillin-streptomycin and 0.5 mM GlutaMax (Thermo Fisher) supplemented with 2% B-27 (Thermo Fisher) and 0.5% FBS (Hyclone). All procedures were conducted according to the guidelines and protocols for rodent experimentation approved by the Institutional Animal Care and Use Committee of DGIST.

Animals

All mice were on a C57BL/6N background, produced by backcrossing with C57BL/6N wild-type mice (purchased from Jackson Research Laboratory) for more than six generations. All mice were maintained and handled in accordance with protocols approved by the Institutional Animal Care and Use Committee of DGIST under standard, temperature-controlled laboratory conditions, or in an enriched environment with free access to tunnels, mazes, climbing materials, and running wheels. Mice were kept on a 12:12 light/dark cycle (lights on at 7:00 am), and received water and food *ad libitum.* Npas4 floxed KO (Npas4$^{f/f}$) mice were previously described (Lin et al., 2008). *Sst-ires*-Cre mice (013044, Jackson Research Laboratories) were gifted from Dr. Eunjoon Kim (KAIST, Korea). Littermate offspring of heterozygous matings were used for all comparative experiments. All experimental procedures were performed on 5∼12-week-old male mice. Pregnant rats purchased from Daehan Biolink were used *in vitro* for dissociated cultures of hippocampal neurons.

METHOD DETAILS

Construction of expression vectors

1. IQSEC3. The shRNA lentiviral expression vector against mouse *Iqsec3* (GenBank accession number: NM_207617.1) was constructed by annealing, phosphorylating, and cloning oligonucleotides targeting mouse *Iqsec3* (5′-ACA TCA GAC CAT CGG CCA CGA CATT A-3′) into *Xho*I and *Xba*I sites of the L-315 vector [see Ko et al., 2011 for a schematic diagram of the L-315 vector]. The shRNA AAV against mouse *Iqsec3* (GenBank accession number: NM_207617.1) was constructed by annealing, phosphorylating, and cloning oligonucleotides targeting mouse *Iqsec3* (5′-GAA CTG GTG GTA GGC ATC TAT GAG A-3′) into *Avr*II and *EcoR*I sites of the pAAV-Ef1α-DSE-mCherry-PSE vector (Addgene). DIO-rat *Iqsec*3 WT and E749A fragments were PCR amplified and subcloned into the pAAV-hSyn-DIO-mCherry vector at *Nhe*I sites. *2*. Others. The shRNA lentiviral expression vector against *Bdnf* was constructed by annealing, phosphorylating, and cloning oligonucleotides targeting rat *Bdnf* (GenBank accession number: AY559250; 5′-ACA TCA GAC CAT CGG CCA CGA CATT A-3′) into the *Xho*I and *Xba*I sites of the L-315 vector. The shRNA lentiviral expression vector against *Npas4* was constructed by annealing, phosphorylating, and cloning oligonucleotides targeting rat *Npas4* (5′-GGT TGA CCC TGA TAA TTT A-3′) into the *Xho*I and *Xba*I sites of the L-315 vector (Yun et al., 2013). AAV encoding human *NPAS4* (GenBank accession number: NM_178864.4) were generated by amplification of the full-length region by PCR and subsequent subcloning into the pAAV-hSynI-DIO-mCherry vector at *Nhe*I sites. *3*. Previously published reagents. The following constructs were as previously described: pcDNA3.1-Myc-Npas4 [a gift from Dr. Yingxi Lin] (Lin et al., 2008); L-315 rat shIQSEC3, pAAV$_{2/9}$-Cre-IRES-EGFP and pAAV$_{2/9}$-ΔCre-IRES-EGFP (Xu and Südhof, 2013); pFSW-Cre and pFSW-ΔCre (Ko et al., 2011); pAAV$_8$-DIO-hM4Di-mCherry (Cat #: 50475; Addgene), pAAV$_8$-DIO-hM3Dq-mCherry (a gift from Dr. Minmin Luo) (Li et al., 2018) and pAAV$_8$-hSyn-DIO-mCherry (Cat #: 50459; Addgene).

Antibodies

The following commercially available antibodies were used: goat polyclonal anti-EGFP (Rockland), goat polyclonal anti-Npas4 (Abcam), mouse monoclonal anti-parvalbumin (clone PARV-19; Swant), mouse monoclonal anti-somatostatin (clone YC7; Millipore), rabbit polyclonal anti-cholecystokinin-8 (ImmunoStar), mouse monoclonal anti-GAD67 (clone 1G10.2; Millipore), rabbit polyclonal anti-VGAT (Millipore), rabbit polyclonal anti-GABA$_A$ receptor γ2 (Synaptic Systems), mouse monoclonal anti-gephyrin (clone 3B11; Synaptic Systems), mouse monoclonal anti-gephyrin (clone mAb7a; Synaptic Systems), rabbit polyclonal anti-pERK1/2 (Cell Signaling Technologies) and rabbit monoclonal anti-c-Fos (clone 9F6; Cell Signaling). The following antibodies were previously described: rabbit polyclonal anti-IQSEC3 [JK079] (Um et al., 2016); guinea pig polyclonal anti-IQSEC3/SynArfGEF [a gift from Dr. Hiroyuki Sakagami] (Fukaya et al., 2011); and rabbit polyclonal anti-Npas4 [a gift from Dr. Michael Greenberg] (Bloodgood et al., 2013).

Iqsec3 promoter-luciferase reporter analysis

A DNA fragment bracketing the proximal promoter and transcription start site of the *Iqsec3* gene (–280 to +36) was PCR-amplified from mouse genomic DNA and subcloned into the pGL3-Basic vector (Promega). Full-length mouse Npas4 cDNA was subcloned in pcDNA3 (GIBCO-Invitrogen). For luciferase assays, 5 × 10^4 HEK293T cells or cultured hippocampal neurons in 24-well plates were transfected with an Npas4 expression vector and reporter plasmid using iN-fect (iNtRON Biotechnology; for HEK293T cells) or CalPhos (Clontech; for cultured hippocampal neurons). Cells were harvested after 48 hours and analyzed for luciferase activity as described by the manufacturer (Promega).

Electrophoretic mobility shift assay

Full-length mouse Npas4 cDNA was subcloned into the pFASTBAC1 vector containing an N-terminal FLAG-tag, and baculovirus was generated according to the manufacturer's instructions (Thermo Fisher). After baculovirus infection into Sf9 insect cells, Npas4 protein was affinity purified on M2 agarose (Sigma) as described previously (Kim et al., 2009). An oligonucleotide containing the consensus sequence for Npas4 binding (5′-CGG GAA GCA GGG TTC CTC ACG AAG CCC AGA GGT GGG AGG TGG-3′) and its point mutant (5′-CGG GAA GCA GGG TTC CTA AAA AAG CCC AGA GGT GGG AGG TGG-3′; mutated nucleotides are underlined) within the *Iqsec3* proximal promoter region were end-labeled using polynucleotide kinase and [γ-^{32}P]ATP and then annealed to complementary oligonucleotides. Reactions containing purified Npas4 protein in 19 μl of reaction buffer (10 mM Tris-Cl pH 7.5, 5 mM $MgCl_2$, 1 mM EDTA, 50 mM K-glutamate, 1 mM DTT and 5% glycerol) supplemented with 25 ng/μl poly (dI-dC) were pre-incubated on ice for 15 minutes. After addition of 1 μl of ^{32}P-labeled probe containing approximately 3 ng of oligonucleotide duplex, reactions were incubated on ice for 30 minutes. Protein in samples were resolved by electrophoresis at 4°C on 6% polyacrylamide gels in 0.25x TBE buffer and subjected to autoradiography.

Chromatin immunoprecipitation assays

Cultured cortical neurons at DIV14 were incubated with or without 55 mM KCl for 6 hours. ChIP analyses were performed according to the manufacturer's instruction (Millipore). Briefly, cells were crosslinked by treating with 1% formaldehyde at 37°C for 10 minutes. After sonicating cells in lysis buffer, cell lysates were subjected to immunoprecipitated by incubating overnight with anti-Npas4 antibodies at 4°C. Protein A agarose was then added and bead were further incubated at 4°C for 4 hours. After extensively washing beads with wash buffer, immunoprecipitated complexes were eluted with elution buffer and protein-DNA complexes were dissociated by incubating overnight at 65°C. DNA was purified by phenol/chloroform extraction, and DNA enrichment was assessed by qPCR analysis. Detailed information about primers used for quantitative PCR is provided in Table S1.

Chemicals

6-Cyano-7-nitroquinoxaline-2,3-dione (CNQX; Cat #: C127), DL-2-Amino-5-phosphonopentanoic acid (AP-V; Cat #: A5282), 2,2,2-tribomoethyl alcohol (Cat #: T4840-2), and Tert-amylalcohol (Cat #: 24048-6), and kainic acid (Cat #: K0250) were purchased from Sigma. KCl (Cat #: 7447-40-7) was purchased from Thermo Fisher Scientific.

Neuron culture, transfections, imaging, and quantitation

Cultured hippocampal neurons were prepared from E18 rat brains, as previously described (Um et al., 2020), cultured on coverslips coated with poly-D-lysine (Sigma), and grown in Neurobasal medium supplemented with B-27 (Thermo Fisher), 0.5% FBS (WELGENE), 0.5 mM GlutaMAX (Thermo Fisher), and sodium pyruvate (Thermo Fisher). For KD experiments in cultured neurons, hippocampal neurons were transfected with L-315 alone (Control), or indicated shRNA expression vector using a CalPhos Transfection Kit (Takara) at DIV8 and immunostained at DIV14. For immunocytochemistry, cultured neurons were fixed with 4% paraformaldehyde/4% sucrose, permeabilized with 0.2% Triton X-100 in phosphate buffered saline (PBS), immunostained with the indicated primary antibodies, and detected with the indicated Cy3- and fluorescein isothiocyanate (FITC)-conjugated secondary antibodies (Jackson ImmunoResearch). Images were acquired using a confocal microscope (LSM780, Carl Zeiss) with a 63 x objective lens; all image settings were kept constant. Z stack images were converted to maximal intensity projection and analyzed to obtain the size, intensity, and density of puncta immunoreactivities derived from marker proteins. Quantification was performed in a blinded manner using MetaMorph software (Molecular Devices).

Quantitative RT-PCR

Cultured rat cortical neurons were infected with recombinant lentiviruses at DIV3 and harvested at DIV10 for qRT-PCR using SYBR green qPCR master mix (Takara). Total RNA was extracted from rat cortical neurons using the TRIzol reagent (Invitrogen) according to the manufacturer's protocol. Briefly, one well of a 12-well plate of cultured neurons was harvested and incubated with 500 μL of TRIzol reagent at room temperature for 5 minutes. After phenol-chloroform extraction, RNA in the upper aqueous phase was precipitated. cDNA was synthesized from 500 ng of RNA by reverse transcription using a ReverTra Ace-α kit (Toyobo). Quantitative PCR was performed on a CFX96 Touch Real-Time PCR system (BioRad) using 1 μL of cDNA. The ubiquitously expressed β-actin was used as an endogenous control. The sequences of the primer pairs used are as follows: rat *Iqsec3*, 5′-GGA GCA GAT TCG GAT AGA ATG G-3′ (forward) and 5′–GGG TGA TCC TTG CTT TGA CT-3′ (reverse); rat *Npas4*, 5′-GAG GCT GGA CAT GGA TTT ACT–3′ (forward) and 5′-CCT GGG TGT TTT CAG AGT TTA G-3′ (reverse).

AAV production, stereotactic surgery and virus injection

Recombinant AAVs were packaged with pHelper and AAV1.0 capsids for high efficiency. HEK293T cells were cotransfected with pHelper and pAAV1.0, together with $pAAV_{2/9}$-ΔCre-IRES-EGFP, $pAAV_{2/9}$-Cre-IRES-EGFP, pAAV-EF1α-DIO-DSE-mCherry-PSE-shIQSEC3, pAAV-hSyn-DIO-mCherry, pAAV-hSyn-DIO-IQSEC3 WT-mCherry, pAAV-hSyn-DIO-IQSEC3 E749A-mCherry, pAAV-hSyn-DIO-hNpas4-mCherry, pAAV-hSyn-DIO-hM4Di-mCherry, and pAAV-hSyn-DIO-hM3Dq-mCherry. Cells were harvested 72–108 hours post transfection; after adding 0.5 M EDTA to the media, cells were washed three times with PBS, and collected by centrifugation. Cells were then resuspended in PBS and lysed by subjecting them to four freeze-thaw cycles in an ethanol/dry ice bath (7 minutes each) and 37°C water bath (5 minutes). Lysates were centrifuged and supernatants were collected and incubated with a solution containing 40% poly(ethylene glycol) (Sigma) and 2.5 M NaCl on ice for 1 hour and centrifuged at 2000 rcf for 30 minutes. The pellets were resuspended in HEPES buffer (20 mM HEPES pH 8.0, 115 mM NaCl, 1.2 mM $CaCl_2$, 1.2 mM $MgCl_2$, 2.4 mM KH_2PO_4), mixed with chloroform, and centrifuged at 400 rcf for 10 minutes. The supernatant was collected and concentrated using Amicon Ultra Centrifugal Filters (0.5 ml, 3K MWCO; Millipore). Viruses were assessed for infectious titer by RT-PCR, and used for infections at 1×10^{10}–10^{11} infectious units/μl. For stereotactic delivery of recombinant AAVs, 6–8-week-old C57BL/6N mice were anesthetized by inhalation of isoflurane (3–4%) or intraperitoneal injection of 2% Avertin solution (2,2,2-tribromoethyl alcohol dissolved in Tert-amylalcohol (Sigma)) dissolved in saline, and secured in the stereotactic apparatus. Viral solutions were injected with a Hamilton syringe using a Nanoliter 2010 Injector (World Precision Instruments) at a flow rate of 100 nl/min (injected volume, 0.6 μl). The coordinates used for stereotactic injections into mice are as follows: hippocampal CA1 injections (AP −3.2 mm, ML ± 3.6 mm, and DV 3.8 mm). Each injected mouse was returned to its home cage and used for immunohistochemical analyses, electrophysiological recordings or behavioral analyses after 2–4 weeks.

Activity alteration protocols

1. Environmental enrichment

Male $Npas4^{f/f}$ mice (P28–P30) injected with the indicated AAVs into the CA1 region were kept for 4 weeks and then exposed to an enriched environment for 4–5 days before functional analyses. The enriched environment consisted of a large cage containing a running wheel, hut, tunnel and several other novel objects, as previously described (Sztainberg and Chen, 2010).

2. Induced seizure protocol

Seizures were induced by intraperitoneal administration of 11–12-week-old male mice with KA (20 mg/kg); saline injection was used as a control. Mice were decapitated 3 hours after injection, and the injected mouse brains were prepared immediately for further analyses.

RNAscope assay

Frozen sections (14-μm thick) were cut coronally through the hippocampal formation and thaw-mounted onto Superfrost Plus microscope slides (Advanced Cell Diagnostics). Sections were fixed in 4% formaldehyde for 15 minutes, dehydrated in increasing concentrations of ethanol for 5 minutes, air-dried, and then pretreated with protease for 30 minutes at room temperature. For RNA detection, sections were incubated in different amplifier solutions in a HybEZ hybridization oven (Advanced Cell Diagnostics) at 40°C. Synthetic oligonucleotides complementary to the sequence corresponding to nucleotide residues 697–1045 of NM-001033354.3 (Mm–*Iqsec3*–tv1), 1908–3117 of NM-001033354.3 (Mm-*Iqsec3*–C2), 793-1795 of NM_153553.4 (Mm-*Npas4*-C2), and 18-407 of NM_009215.1 (Mm-*Sst*-C3) (Advanced Cell Diagnostics) were used as probes. The labeled probes were conjugated to Alexa Fluor 488, Altto 550 or Altto 647, after which labeled probe mixtures were hybridized by incubating with slide-mounted sections for 2 hours at 40°C. Nonspecifically hybridized probes were removed by washing the sections three times for 2 minutes each with 1X wash buffer at room temperature, followed by incubation with Amplifier 1-FL for 30 minutes, Amplifier 2–FL for 15 minutes, Amplifier 3–FL for 30 minutes, and Amplifier 4 Alt B–FL for 15 minutes at 40°C. Each amplifier was removed by washing with 1X wash buffer for 2 minutes at room temperature. The slides were imaged using a confocal microscope (LSM800 microscope, Zeiss) with a 40 x objective lens; all images settings were kept constant. Quantification was performed in a blinded manner using MetaMorph (Molecular Devices).

Immunohistochemistry and imaging

Mice were anaesthetized and immediately perfused, first with PBS for 3 minutes, and then with 4% paraformaldehyde for 5 minutes. Brains were dissected out, fixed in 4% paraformaldehyde overnight, and then incubated with 30% sucrose (in PBS) overnight, and sliced into 30 μm-thick coronal sections using a vibratome (Model VT1200S; Leica Biosystems) or a cryotome (Model CM-3050-S; Leica Biosystems). Sections were permeabilized by incubating with 0.3% Triton X-100 in PBS containing 5% bovine serum albumin and 5% horse serum for 1 hour. For immunostaining, sections were incubated for 8–12 hours at 4°C with primary antibodies diluted in the same blocking solution. The following primary antibodies were used: anti-Npas4 (1: 300), anti-IQSEC3 (JK079; 2 μg/ml), anti-GAD67 (1: 100), anti-VGAT (1: 500), anti-$GABA_AR\gamma2$ (1: 500), anti-PV (1: 500), anti-CCK (1: 100), anti-SST (1: 50), anti-c-Fos (1: 500), and anti-pERK1/2 (1: 100). Sections were washed three times in PBS and incubated with appropriate Cy3- or FITC-conjugated secondary antibodies (Jackson ImmunoResearch) for 2 hours at room temperature. After three washes with PBS, sections were mounted onto glass slides (Superfrost Plus; Fisher Scientific) with Vectashield mounting medium (H-1200; Vector Laboratories). Z stack images (6–8 images, 2 μm thickness) were acquired in standard mode with a laser-scanning confocal microscope (LSM800 with Airyscan mode; Zeiss) equipped with a 20x objective (0.156 mm/pixel; x-y dimension 1024 × 1024) and processed using the maximum intensity projection function in

Zen2.6 software (Zeiss). For quantification, a region of interest was manually selected, then calibrated and thresholded using the Length Calibration and Threshold (100 minimum and 255 maximum) functions, respectively, of MetaMorph Software (Molecular Devices) to remove background signals. Synaptic puncta in the size range 0.1–10 μm^2 were counted using the Histogram function.

In utero electroporation

After anesthetizing pregnant ICR mice at 15 *days post coitum* (d.p.c) with an intraperitoneal injection of pentobarbital sodium (64.8 mg/kg), uterine horns were exposed through a longitudinal incision (~2 cm) in the abdomen. Approximately 1 μL of a solution containing 1 mg/ml pCAGGS-EGFP cDNA, 1.5 mg/ml L-315 shIQSEC3 and 0.01% Fast Green in PBS, or 1 mg/ml pCAGGS-EGFP cDNA, 1.5 mg/ml L-315 control shRNA and 0.01% Fast Green in PBS was injected into the lateral ventricle of each embryo through a glass capillary electrode. The head of each embryo was placed between tweezer-type electrodes (CUY650P5; NEPA Gene). The anode of the electrode was placed on the injection side for transfection of hippocampal CA1 pyramidal neurons. Square electric pulses (35 V, 50 ms) were administered four times at 1 Hz using an electroporator (CUY21; NEPA Gene). The uteri were returned to the peritoneal cavity, and the incisions were sutured. Operated mice were returned to their home cages and subsequently allowed to deliver naturally. The transfected pups were identified at P0 by visualizing EGFP signals through the scalp using an LED penlight (Handy Blue; Reryon).

Electrophysiology

1. Hippocampal CA1 pyramidal neuron electrophysiology

Electrophysiological recordings in brain slices were obtained as previously described (Um et al., 2014). Briefly, P28–34 mouse brains were removed and immediately immersed for 2 min in ice-cold slicing solution (85 mM NaCl, 75 mM sucrose, 25 mM glucose, 24 mM $NaHCO_3$, 1.25 mM NaH_2PO_4, 2.5 mM KCl, 4 mM $MgCl_2$, and 0.5 mM $CaCl_2$) saturated with 95% O_2/5% CO_2. Chilled brains were trimmed coronally with razor blades, bonded to a metal platform after dissecting out the olfactory bulb and cerebellum, and then placed in the chamber of a vibratome (Campden 7000smz) filled with ice-cold slicing solution. Coronal sections (0.35 mm thick) were prepared and transferred to a chamber containing artificial cerebrospinal fluid (ACSF; 126 mM NaCl, 2.5 mM KCl, 1.25 mM NaH_2PO_4, 26 mM $NaHCO_3$, 10 mM glucose, 2 mM $CaCl_2$, and 2 mM $MgCl_2$) for recovery, then initially incubated at 32°C for 30 min followed by incubation at room temperature for 1 h. For whole-cell voltage-clamp recordings in acute cortical slices, patch pipettes (4–8 MΩ) were filled with a 290-mOsm internal solution with the composition, 130 mM Cs-gluconate, 6 mM CsCl, 10 mM HEPES (pH 7.2), 1 mM EGTA, 2.5 mM $MgCl_2$, 2 mM Mg-ATP, 0.5 mM Na-GTP, and 10 mM Na-phosphocreatine. All recordings were performed in ACSF at 28–30°C under a fluorescence microscope (BX50-WI, Olympus). mEPSC and mIPSC recordings were performed with voltage clamped at −60 (reversal potential of $GABA_A$ receptor) or 0 mV (reversal potential of AMPA receptor) in the presence of 1 μM tetrodotoxin (TTX), included to block action potential-evoked responses. Membrane statistics in each experiment were monitored by collecting three 1-min traces with a −2 mV voltage step between each trace. Paired-pulse ratios (PPRs) of IPSCs were assessed at 50-ms inter-stimulus intervals. Evoked IPSCs were recorded in the presence of 10 μM 6,7-dinitroquinoxaline-2,3-dione (DNQX; Abcam) and 25 μM AP5 (Abcam). For all whole-cell recordings, membrane statistics were monitored after each trace. Cells for whole-cell recording were rejected if Ra was ≥ 25 MΩ, or if Ra or Rm changed by 25% or more over the course of the experiment. All recordings were digitized at 10 kHz and filtered at 2 kHz. Recordings were monitored with an EPC10 double USB patch-clamp amplifier (HEKA) and analyzed offline using the Mini Analysis program (Synaptosoft).

2. Hippocampal CA1 somatostatin interneuron electrophysiology

Whole-cell voltage-clamp recordings were obtained from acute brain slices. Brain slices were transferred to a recording chamber and perfused with a bath solution of aerated (O_2 95%/CO_2 5% mixed gas) artificial cerebrospinal fluid (aCSF) consisting of 124 mM NaCl, 3.3 mM KCl, 1.3 mM NaH_2PO_4, 26 mM $NaHCO_3$, 11 mM D-glucose, 2.5 mM $CaCl_2$, and 1.5 mM $MgCl_2$ at 28–30°C. For measuring postsynaptic currents, patch pipettes (open pipette resistance, 3–5 MΩ) were filled with an internal solution consisting of 145 mM CsCl, 5 mM NaCl, 10 mM HEPES, 10 mM EGTA, 4 mM Mg-ATP, and 0.3 mM Na-GTP. Whole-cell recordings of mIPSCs were performed on CA1 *stratum oriens* SST^+ interneurons, voltage clamped at −70 mV, and currents were pharmacologically isolated by bath application of 50 μM DL-APV (Sigma), 10 μM CNQX (Sigma), and 1 μM TTX (Tocris). Whole-cell recordings of mEPSCs were performed on CA1 *stratum oriens* SST^+ interneurons, voltage clamped at −70 mV, and currents were pharmacologically isolated by bath application of 50 μM picrotoxin (Tocris) and 1 μM TTX (Tocris). For measuring action potential firing, patch pipettes were filled with an internal solution consisting of 130 mM K-gluconate, 20 mM KCl, 0.2 mM EGTA, 10 mM HEPES, 4 mM Mg-ATP, 0.3 mM Na-GTP, 10 mM disodium phosphocreatine. Action potentials fired in 10 s intervals during incremental injection of current (−50 pA to 200 pA). For DREADD validation experiments, 10 μM CNO was bath-applied, after which 1 s, 200-pA current injections were delivered into CA1 *stratum oriens* SST^+ interneurons and action potential firing was recorded. Electrophysiological data were acquired using pCLAMP software and a MultiClamp 700B (Axon Instruments), and were digitized using an Axon DigiData 1550B data acquisition board (Axon Instruments). Data were sampled at 10 kHz and filtered at 4 kHz. Data were discarded if the series resistance was greater than 30 MΩ, or the series resistance differed by more than 20%.

Mouse behavioral tests

Male *Npas4*$^{f/f}$ mice (5–6 weeks old) crossed with the *Sst-ires*-Cre driver line were injected with the indicated AAVs were used for all behavioral tests. Tests were performed in the following order: Y-maze, open-field, novel object-recognition, elevated-plus maze, and

forced swim test. Light-dark transition and novelty-suppressed feeding tests were performed with separate cohorts. Mice were excluded for quantitative analyses if one or both of the injections were off-target, as demonstrated by *post hoc* immunostaining after behavioral analyses. *1. Y-maze test.* A Y-shaped white acrylic maze with three 40-cm–long arms at a 120° angle from each other was used. Mice were introduced into the center of the maze and allowed to explore freely for 8 minutes. An entry was counted when all four limbs of a mouse were within the arm. The movement of mice was recorded by a top-view infrared camera, and analyzed using EthoVision XT 10.5 software (Noldus). *2. Open-field test.* Mice were placed into a white acrylic open-field box (40 × 40 × 40 cm), and allowed to freely explore the environment for 30 minutes in dim light (< 20 lux). The traveled distance moved and time spent in the center zone of freely moving mice were recorded by a top-view infrared camera, and analyzed using EthoVision XT 10.5 software (Noldus). *3. Novel object-recognition test*. An open field chamber was used in this test. Mice were habituated to the chamber for 10 minutes. For training sessions, two identical objects were placed in the center of the chamber at regular intervals, and mice were allowed to explore the objects for 10 minutes. After the training session, mice were returned to their home cage for 12 hours. For novel object-recognition tests, one of the two objects was exchanged for a new object, placed in the same position of the chamber. Mice were returned to the chamber and allowed to explore freely for 10 minutes. The movement of mice was recorded by infrared camera, and the number and duration of contacts were analyzed using EthoVision XT 10.5 (Noldus). *4. Elevated plus-maze test.* The elevated plus-maze is a plus-shaped (+) white acrylic maze with two open arms (30 × 5 × 0.5 cm) and two closed arms (30 × 5 × 30 cm) positioned at a height of 75 cm from the floor. Light conditions around open and closed arms were ~300 and ~30 lux, respectively. For the test, mice were introduced into the center zone of the elevated plus-maze and allowed to move freely for 5 minutes. All behaviors were recorded by a top-view infrared camera, and the time spent in each arm and the number of arm entries were measured and analyzed using EthoVision XT 10.5 software (Noldus). *5. Light-dark transition test.* The apparatus consists of two compartments—a dark chamber (~2 lux) and a brightly illuminated chamber (390 lux)—divided by a partition with a hole to allow the mouse to select between the two chambers. For the test, a mouse was transferred to the testing box and allowed to move freely between the two compartments for 10 minutes. The number of entries and time spent in the lighted box were recorded by a top-view infrared camera and were analyzed using EthoVision XT 10.5 software (Noldus). *6. Novelty-suppressed feeding test.* An open-field plastic box (40 × 40 × 40 cm) with standard bedding was used for the test, and a food platform with food pellets was placed in the center of the chamber. Twenty-four hours before behavioral testing, mice were food-deprived in their home cage, then transferred to the testing box and allowed to move and eat food pellets freely for 10 minutes. After the testing, mice were transferred to their home cage and their food consumption was measured for 5 min. All behaviors were recorded using a top-view infrared camera, and feeding latency and the number of feedings was counted manually by inspection of recorded video files. *7. Forced swim test.* Mice were individually placed in a glass cylinder (15 × 30 cm) containing water (24 ± 1°C; depth, 15 cm). All mice examined were forced to swim for 6 minutes, and the duration of immobility was recorded and measured during the final 4 minutes of the test. The latency to immobility from the start of the test (delay between the start of the test and appearance of the first bout of immobility, defined as a period of at least 1 s without any active escape behavior), and the duration of immobility (defined as the time not spent actively exploring the cylinder or trying to escape from it) were measured. Immobility time was defined as the time the mouse spent floating in the water without struggling, making only minor movements that were strictly necessary to maintain its head above water.

Chemogenetic manipulation with DREADDs

Male *Sst-ires*-Cre and SST-*Npas4*–KO mice (5–6 weeks old) were anesthetized by intraperitoneal injection of a 2% Avertin solution (2,2,2-tribromoethyl alcohol dissolved in tert-amyl alcohol [Sigma]) dissolved in saline, and secured in a stereotactic apparatus. Mice were then injected into the hippocampal CA1 region (relative to bregma: AP −3.2 mm, ML ± 3.6 mm, DV 3.8 mm) with 200 nL of AAV_8-hSyn-DIO-hM4Di(Gi)-mCherry, AAV_8-hSyn-DIO-hM3D(Gq)-mCherry or AAV_8-hSyn-DIO-mCherry (Control). After allowing 2 weeks to recover from surgery, a solution containing the designer receptor ligand, Clozapine-N-oxide (CNO) (3 mg/kg body weight), or vehicle (saline) was administered into the indicated AAV-injected mice by a single IP injection 30 minutes before the start of behavioral experiments.

QUANTIFICATION AND STATISTICAL ANALYSIS

Data analysis and statistics

Data are expressed as the mean ± SEM. All experiments were repeated at least three times independently, and data were statistically evaluated using a Mann-Whitney *U* test, Shapiro-Wilk normality test, analysis of variance (ANOVA) followed by Tukey's *post hoc* test, Kruskal-Wallis test (one-way ANOVA on ranks), Welch's test, or one-way ANOVA with Bonferroni's post hoc test (for behavior experiments), as indicated in each figure legend and listed in Table S3. Prism7 (GraphPad Software) was used for analysis of data and preparation of bar graphs. *P* values < 0.05 were considered statistically significant (individual *p* values are presented in Table S3).